Mathematical modeling of the circadian clock in oncogene induced senescence

Kaiyang Zhang

Thesis to obtain the Master of Science Degree in

Biotechnology

Advisors: Dr. Angela Moreira Borralho Relógio
Prof. João Miguel Raposo Sanches

Examination Committee

Chairperson: Prof. Isabel Maria de Sá Correia Leite de Almeida
Advisor : Prof. João Miguel Raposo Sanches
Member of the Committee: Prof. Miguel Nobre Parreira Cacho Teixeira

September 2015

Acknowledgements

The work presented in the thesis has been carried out in the Institute for Theoretical Biology at the Charité Medical University of Berlin. I would like to express my gratitude towards all the persons and organizations that help me during the process and made this work possible.

First, I would like to thank the Consortium of the Erasmus Mundus Master program in Systems Biology (euSysBio) for giving me the opportunity to pursue a Master's degree in Systems and Computational Biology and generously support my studies with scholarship.

At the same time, I am especially grateful to my supervisor Dr. Angela Relógio for her support and valuable guidance throughout my work, for her motivation, enthusiasm, and immense knowledge. I want to further thank my lab mates for their support, in particular, I want to thank Jeannine Mazuch, Mónica Abreu and Luise Fuhr for providing me with their experimental data and for guiding me through the experimental part of the work. I thank Anuprabha Bhargava for willingness to discuss all kinds of bioinformatics related issues.

My sincere thank also goes to Prof. Isabel Sá-Correia and Prof. Erik Aurell, our program coordinators at Instituto Superior Técnico (IST) and Royal Institute of Technology (KTH) for their constant support throughout my master's studies. I want to thank my institutional advisor Prof. João Sanches for his help and treasured feedback and comments regarding my thesis. Furthermore, I also want to thank all the members of the jury for having agreed to judging this thesis.

Finally, I would like to thank my parents and my friends for their love and support.

Resumo

O relógio circadiano é um sistema interno de controlo e geração tempo presente na maioria dos organismos, sendo responsável pelo seu ritmo comportamental e fisiológico, e com uma periocidade de aproximadamente 24 horas. A desregulação do relógio circadiado pode levar à perturbação de importantes processos celulares envolvidos no desenvolvimento tumoral, nomeadamente a regulação do ciclo cellular. Um modelo matemático do relógio circadiano em mamiferos foi previamente estabelecido pelo nosso grupo, no qual estão representados os principais mecanismos circadianos através de dois *feedback loops* negativos interligados: o PERs/CRYs (PC) loop e o RORs/Bmal1/REV-ERBs (RBR) loop.

Neste projecto, o modelo matemático previamente desenvolvido para o relógio circadiano em mamíferos foi alargado a outros genes e vias de tranmmissaõ de sinais considerados cruciais na regulação do ciclo celular por oncogenes, nomeadamente *Myc*, *Wee1*, vias INK4a-CDK/CycD-Rb-E2F e via ARF-MDM2-p53, com o objectivo de perceber a interacção entre o relógio circadiano em mamiferos e a senescencia induzida por oncogenes. O novo modelo foi usado para interpreter os resultados experimentais obtidos pelo nosso grupo em fibroblástos embrionários de ratinho (MEF), nos quais foram observados fenotipos opostos para os periodos circadianos aquando da superexpressão de RAS em *wild type* e INK4a/ARF$^{-/-}$ MEFs. Os perfis de expressão *in silico* dos genes do relógio circadiano obtidos pelas simulações no novo modelo são comparáveis e validam os resultados experimentais bem como as análises de microarrais realizadas no grupo. Adicionalmente, algumas previsões feitas pelo novo modelo serão futuramente validadas experimentalmente.

Palavras-chave: biologia de sistemas, relógio circadiano, senescencia induzida por oncogenes, modelos matemáticos, equação diferencial ordinária

Abstract

The circadian clock is an internal timing system present in most living organisms, which is responsible for the behavioral and physical rhythms with a periodicity of approximately 24 hours. Deregulation of circadian clock may disrupt major cellular processes involved in tumor progression, including the cell cycle regulation. A mathematical model of the mammalian circadian clock has already been established in our group, representing the core of circadian mechanisms by two interconnected negative feedback loops: the PERs/CRYs (PC) loop and the RORs/Bmal1/REV-ERBs (RBR) loop.

In the present project, the previously developed mathematical model for the mammalian core-clock system was extended to output genes and pathways which are considered to be crucial in the regulation of oncogene-induced senescence, namely *Myc*, *Wee1*, INK4a-CDK/CycD-Rb-E2F pathway and ARF-MDM2-p53 pathway, aiming to gain insights into the crosstalks between mammalian circadian clock and oncogene-induced senescence. The newly extended model was used to interpret the experimental data produced in a mouse embryonic fibroblast (MEF) system in our group, where upon RAS overexpression wild type and INK4a/ARF$^{-/-}$ MEFs showed opposite circadian period phenotypes. In *silico* expression profiles of core-clock genes obtained from simulations with the extended model were compared with and verified by experiments and microarray data analysis in our group. Furthermore, a set of predictions has been made with the extended model and will be assessed against experimental data in the future.

Keywords: systems biology, circadian clock, oncogene-induced senescence, mathematical modeling, ordinary differential equations

Contents

List of figures VI

List of tables VIII

List of abbreviations IX

1. Introduction 10

1.1 The mammalian circadian clock 10

1.2 The cell cycle and checkpoints 11

1.3 Oncogene-induced cellular senescence. 12

1.4 Crosstalks between circadian clock and oncogene-induced senescence 13

1.4.1 The cell cycle checkpoint genes *Myc* and *Wee1* are regulated by CLOCK/BMAL1 . . . 13

1.4.2 The CDKN2A locus and circadian clock. 13

1.4.2.1 p16/INK4a-CDK4/6-Rb-E2F1 pathway. 14

1.4.2.2 ARF-MDM2-p53 pathway. 15

1.4.3 p21/Cip1 interconnects p53 and Rb. 15

1.5 Existing mathematical models of the mammalian circadian clock. 16

1.6 Aims. 17

2. Materials and methods 19

2.1 Modeling data. 19

2.1.1 Mass action law 19

2.1.2 Michaelis-Menten kinetics and Hill kinetics. 19

2.1.3 Modeling of transcriptional regulation. 20

2.2 Experiment data. 22

2.2.1 Cell culture. 22

2.2.2 Lentivirus production. 22

2.2.3 Lentiviral transduction. 22

2.2.4 Adriamycin treatment 23

2.2.5 Synchronization and measurement of circadian rhythms. 23

2.2.6 Circadian data. 23

3. Results 24

3.1 Experimental data 24

3.2 Model design. 25
3.2.1 Extend the model to *Wee1*, *Myc*, *Ink4a* and *Arf* 28
3.2.2 INK4a-CDK/CycD-Rb-E2F pathway and its regulation of *Bmal*. 30
3.2.3 ARF-MDM2-p53 pathway and its regulation of *Per* 32
3.3 Model analysis. 34
3.3.1 The extended model reproduces essential features of the core circadian system. 34
3.3.2 Simulation of experimental data with the extended model. 36
3.3.3 Comparison between computational predictions and microarray data. 38
3.3.4 Modular analysis. 43
3.3.5 Model predictions. 46
3.3.5.1 Model predictions of circadian phenotypes of $ARF^{-/-}$, $INK4a^{-/-}$, $Rb^{-/-}$, $E2F^{-/-}$ MEFs 46
3.3.5.2 Model prediction of the effect of adriamycin on the period. 48

4. Discussion **50**

References **53**

Appendices **58**

List of figures

Figure 1: Architecture of the mammalian circadian timing system. 10

Figure 2: Model of the cell cycle checkpoints. 12

Figure 3: Oncogenic induction of senescence via INK4a and ARF. 13

Figure 4: Structure of the CDKN2A locus. 14

Figure 5: The PER/NONO complex regulates cellular senescence by activating the transcription of *Ink4a*. 15

Figure 6: Model of the mammalian circadian clock. 17

Figure 7: Project outline. 18

Figure 8: WT and INK4a/ARF$^{-/-}$ MEFs shows opposite morphological phenotypes and circadian phenotypes. 24

Figure 9: Simplified schematic diagram of the extended network. 26

Figure 10: Detailed diagram of the extended network. 27

Figure 11: *Wee1* and *Myc* are regulated by core-clock genes. 28

Figure 12: Detailed diagram of reactions involving *Ink4a* and *Arf*. 29

Figure 13: Detailed reaction diagram of INK4a-CDK/CycD-Rb-E2F pathway and its effect on *Bmal* transcription. 31

Figure 14: Detailed reaction diagram of ARF-MDM2-p53 pathway and its effect on CLOCK/BMAL-mediated transcription of *Per*. 33

Figure 15: Comparison of *in silico* expression profiles of core-clock components obtained from the simulations with the original model and extended model. 35

Figure 16: In *silico* phase data of the extended model fits with data of original model and with known experimental data. 35

Figure 17: In *silico* data of circadian periods and *Bmal* expression profiles of WT and INK4a/ARF$^{-/-}$ systems. 37

Figure 18: In *silico* expression profiles of *Ink4a* over 6 days obtained using the extended model. . . . 38

Figure 19: In *silico* expression profiles of core-clock genes in WT system upon RAS overexpression simulated with the extended model over 6 days. 39

Figure 20: In *silico* expression profiles of core-clock genes in INK4a/ARF$^{-/-}$ system upon RAS overexpression simulated with the extended model over 6 days. 40

Figure 21: In *silico* expression profiles of core-clock genes in WT system upon the knockdown of *Bmal* simulated with the extended model over 6 days. 42

Figure 22: Simplified schematic diagram of the extended network with the INK4a-CDK-Rb-E2F module and the ARF-MDM2-p53 module highlighted. 43
Figure 23: The relevance of Module 1 to period phenotypes. 44
Figure 24: The relevance of Module 2 to period phenotypes. 45
Figure 25: In *silico* expression profiles of *Bmal* and $BMAL_N$ obtained from simulations with the extended model over 3 days. 47
Figure 26: In *silico* and experimental analysis of the effect of adriamycin induction on circadian period. 49
Figure 27: Effect of p53 overexpression on circadian period of MEFs (*in silico*). 52
Figure S1: Simplified schematic diagram of the extended network with references for newly-added links marked. 58

List of tables

Table 1: Comparison of peak phases data obtained from original and extended models. 36

Table 2: Corresponding values of the phases and periods of original and extended models shown in Figure 16B. 38

Table S1: List of Variables. 59

Table S2: List of parameters. 61

Table S3: Robustness analysis. 67

Table S4: Ordinary differential equations for core-clock components. 71

List of abbreviations

ARF: ARF tumor suppressor

$ARF^{-/-}$: ARF knockout

Arntl 1 (Bmal1): Aryl hydrocarbon receptor nuclear translocator-like protein 1

CDK: cyclin-dependent kinase

Clock: Circadian Locomotor Output Cycles Kaput

Cry1, Cry2: Cryptochrome genes

CycD: D-type Cyclin

CycE: E-type Cyclin

DDE: delayed differential equation

DMEM: Dulbecco's Modified Eagle Medium

DNA: Deoxyribonucleic acid

E-box: Enhancer Box

$E2F^{-/-}$: E2F knockout

FBS: fetal bovine serum

$INK4a^{-/-}$: INK4a knockout

$INK4a/ARF^{-/-}$: INK4a and ARF knockout

LTI: linear time-invariant

MAPK: Mitogen-activated protein kinases

Mdm2: Mouse double minute 2 homolog

MEF: mouse embryonic fibroblast

mRNA: messenger RNA

Myc: myelocytomatosis oncogene

ODE: Ordinary differential equation

Per1, Per2, Per3: Period homolog genes

p16/INK4a: cyclin-dependent kinase inhibitor 2A

p53: tumor protein p53

Rb: retinoblastoma protein

$Rb^{-/-}$: Rb knockout

REV-ERBα, REV-ERBβ: Rev-Erb nuclear orphan receptors

Rora, Rorb, Rorc: retinoic acid-related orphan nuclear receptors

RRE: ROR regulatory element

SCN: suprachiasmatic nucleus

Wee1: WEE1 G2 checkpoint kinase

WT: wild-type

1. Introduction

1.1 The mammalian circadian clock

Circadian rhythms are responsible for the oscillations in behavior and physiology that occur with a periodicity of approximately 24 hours. They are ubiquitous phenomena present in most living organisms, from cyanobacteria to humans [1]. Accumulating experimental evidence shows that the circadian clock can influence major cellular processes including the cell cycle regulation [2], DNA damage responses [3] and metabolism [4], which are thought to be important in cancer progression .

Physiological rhythms are controlled by an endogenous circadian timing system. In mammals, these daily-endogenous rhythms are generated by a master clock located in the suprachiasmatic nucleus of the hypothalamus (SCN) that responses to external cues and drives subordinate clocks in peripheral tissues through circadian output pathways [5, 6].

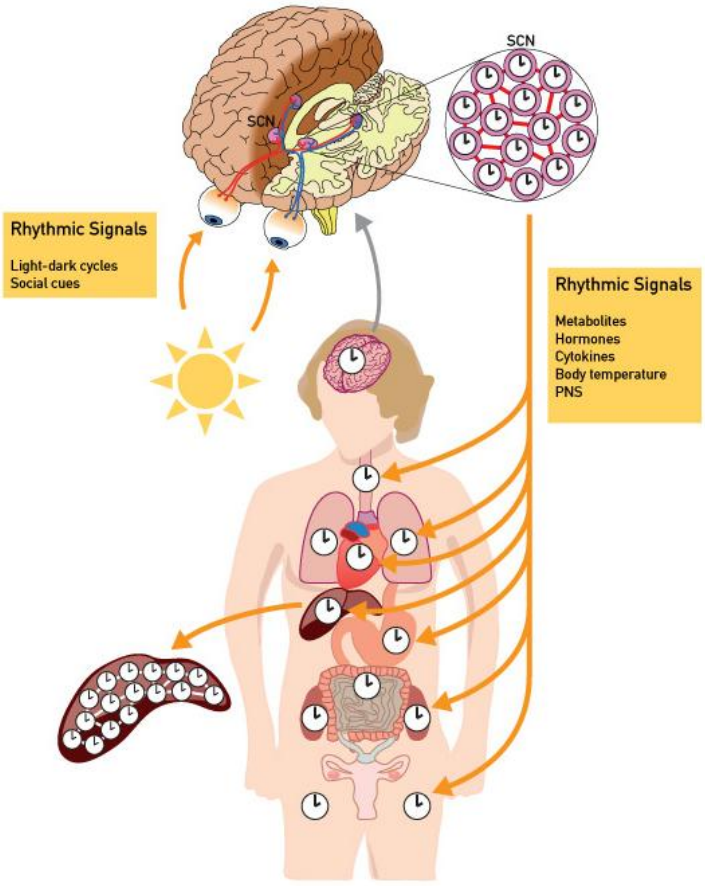

Figure 1: Architecture of the mammalian circadian timing system [7]. The master clock is located in the suprachiasmatic nucleus (SCN) and is entrained by external cues (e.g. light-dark cycles, social cues). It synchronizes the clocks in peripheral organs via metabolic cues, hormones, cytokines and other internal stimuli.

In individual cells, the core of the circadian clock can be represented by two interconnected negative feedback loops: the PERs/CRYs (PC) loop and the RORs/Bmal1/REV-ERBs (RBR) loop,

which can generate oscillations in gene expression with a period of around 24 hours [8, 9]. These two loops are interlocked through a functional heterodimer, CLOCK/BMAL, formed by CLOCK, a basic helix-loop-helix-PAS transcription factor encoded by circadian locomotor output cycles kaput (*Clock*), and BMAL1, the Aryl hydrocarbon receptor nuclear translocator-like protein 1.

It is commonly believed that circadian rhythms are mainly generated by the PC loop, in which the CLOCK/BMAL1 heterodimers can activate the transcription of *Period* homolog genes (*Per1, Per2, Per3*) and Cryptochrome genes (*Cry1, Cry2*) by binding to the E-box *cis*-elements in their promoter regions [10]. Both hypophosphorylated and hyperphosphorylated PER proteins can form repress complexes with CRY proteins in the cytoplasm and then translocate to the nucleus to associate with CLOCK/BMAL1 heterodimers, inhibiting further transcriptional activation. As the cellular concentration of PER and CRY decreases, the repression on CLOCK/BMAL1 is relieved and a new PER/CRY accumulation cycle starts [11]. In the other feedback loop, CLOCK/BMAL1 can activate the retinoic acid-related orphan nuclear receptors (RORa, b, c) and other two nuclear receptors REV-ERBα and REV-ERBβ. In turn, ROR and REV-ERB proteins can modulate the transcription of *Bmal1* by competing for ROR regulatory element (RRE) binding sites in its promoter region [12]. ROR proteins activate the transcription of *Bmal1* while REV-ERBs are inhibitors of *Bmal* [12]. REV-ERBs also influence the PC loop via inhibiting *Crys*. There is evidence showing that the oscillations are not damped when components in the PC loop are overexpressed, which indicated that the RBR loop may act as an independent oscillator instead of a merely auxiliary loop adding robustness to the system [9, 13, 14].

1.2 The cell cycle and checkpoints

The cell cycle is a sequence of biochemical and structural events that occur in a cell between two successive cell divisions [15, 16]. It can be divided into five phases: G0 phase (also called resting phase), the gap in which the cell is quiescent; G1 phase (also called Growth1 phase or Gap1 phase), is a part of cell cycle when mRNAs and proteins are synthesized in preparation for DNA synthesis; S phase (synthesis phase), during which DNA replication occurs; G2 phase (pre-mitotic phase), in which the cell rapidly grows in size and proteins are synthesized for mitosis; M phase (mitotic phase), in which the cell undergoes mitosis and it is divided into two daughter cells [17].

The eukaryotic cell cycle is controlled for failure at three checkpoints: the G1/S checkpoint, the G2/M checkpoint, and the metaphase/anaphase checkpoint:

- G1/S checkpoint: the cell double checks DNA integrity before allowing progress into the S phase and replication of the DNA. It is also the most important checkpoint for regulating senescence decision.

- G2/M checkpoint: this checkpoint prevents the initiation of mitosis before the cell complete DNA replication and the damaged DNA is repaired.

- Metaphase/anaphase checkpoint (also called spindle checkpoint): this checkpoint is activated by the lack of microtubule occupancy and tension at the kinetochores to ensure the proper chromosome distribution [18].

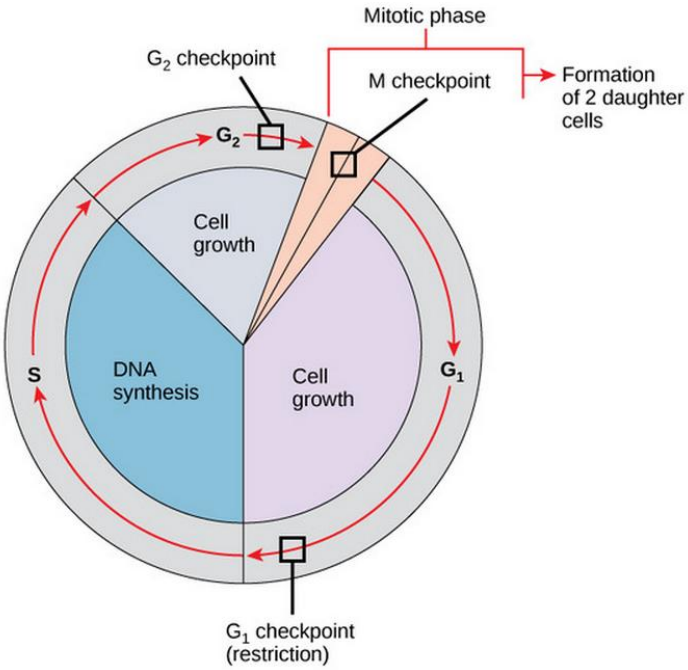

Figure 2: Model of the cell cycle checkpoints. The cell cycle progression is regulated by three checkpoints: at G1 (G1/S) checkpoint, DNA integrity is confirmed; at G2 (G2/M) checkpoint, the completion of DNA replication is confirmed; and M checkpoint ensures the proper chromosome distribution.

The core-clock regulates a next layer of clock-controlled genes which fine-tune several molecular processes from metabolism to the cell cycle. In particular, the cell cycle checkpoint regulators WEE1 (G2/M checkpoint), MYC (G1/S checkpoint) and cyclin D1 (G1/S checkpoint), which have been shown to be circadian regulated by the CLOCK/BMAL1 complex, representing a pathway via which the circadian clock may regulate cancer progression and malignancy [19]. In the present project, we are interested in the interactions between the circadian clock and the cell cycle and its effects on the molecular decisions that lead to cellular senescence.

1.3 Oncogene-induced cellular senescence

Cellular senescence or replicative senescence was initially described as a state of terminal cell cycle arrest that metabolically active cells may enter after a certain, finite number of divisions [20, 21]. Cellular senescence is one of the most important mechanisms to eliminate damaged or stressed cells, which is particularly relevant in aging and cancer, and it is commonly considered to function as an crucial barrier against tumor progression [22]. Multiple stimuli, including telomere shortening, chromatin perturbation, DNA damage, oxidative stress and activation of oncogenes, may lead normal cells into senescense [23] [24]. These stimuli are signaled through different pathways, many of which activate the cyclin-dependent kinase (CDK) inhibitors p16/INK4a, p15/INK4b, p21/WAF1 and p27 [22] and subsequently inhibit the activity of CDK–cyclin complexes resulting in proliferative arrest.

The senescence of normal cells upon overexpression of oncogenes, such as *Ras*, *Myc* and *Raf*, is called oncogene-induced senescence, and it plays an important role in protecting cells from

oncogenic transformation [22, 25]. The ARF-MDM2-p53 and p16/INK4a-RB tumor-suppressor pathways are commonly believed to play essential roles in promoting cellular senescence in response to aberrant *Ras* activation [26].

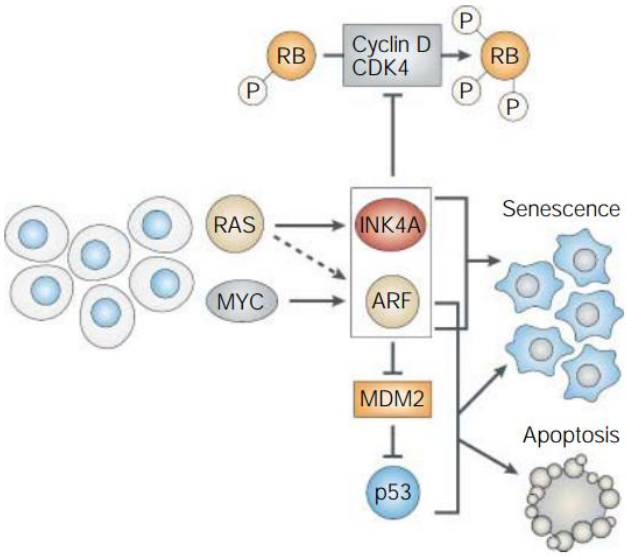

Figure 3: Oncogenic induction of senescence via INK4a and ARF [27]. The aberrant activation of oncogenes (*Ras* and *Myc*) leads to cellular senescence or apoptosis through INK4a-CDK4-Rb pathway and ARF-MDM2-p53 pathway. The constitutively overexpressed RAS induces the expression of INK4a which inhibit the phosphorylation of Rb mediated by CDK4/cyclin D complex and drive cells to senescence. Overexpression of MYC leads to upregulation of ARF, which stabilizes and actives p53 by binding to MDM2 and provokes apoptosis or senescence.

1.4 Crosstalks between circadian clock and oncogene-induced senescence

1.4.1 The cell cycle checkpoint genes *Myc* and *Wee1* are regulated by CLOCK/BMAL1

Myc is an important regulator of the G1/S checkpoint. It promotes the transition from G1 to S phase through the activation of genes encoding proteins of the cyclin-dependent kinase (CDK) complex [28]. Overexpression of *Myc* could drive cell proliferation but also sensitize cells to senescence [29, 30]. The expression of *Myc* is directly repressed by CLOCK/BMAL1 through binding to the cis-acting E-box elements within its promoter region [31].

Wee1, a key component of the G2/M checkpoint, is a kinase phosphorylating the Cyclin-dependent kinase 1 (CDK1). Both mRNA and protein levels of Wee1 are positively regulated by CLOCK/BMAL1 complex through E box-mediated reactions, and its target, CDK1, exhibits rhythmic phosphorylation [32].

1.4.2 The CDKN2A locus and circadian clock

The CDKN2A locus encodes two tumor suppressors: p16/INK4a (hereafter referred as INK4a) and p19/ARF (hereafter referred as ARF). As shown in Figure 4, the two transcripts have different first exons, which are driven from distinct promoters and subsequently spliced to the same second and

third exon [33]. Published data suggests that these two tumor suppressors can mediate the interplay between oncogene-induced senescence and circadian core-clock via the INK4a-CDK4/6-Rb-E2F1 pathway and the ARF-MDM2-p53 pathway, respectively.

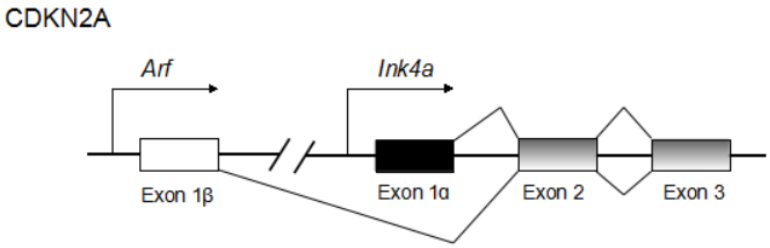

Figure 4: Structure of the CDKN2A locus. *Ink4a* and *Arf* transcripts have distinct first exons, Exon 1α and Exon 1β, respectively, and they share Exon 2 and Exon 3.

1.4.2.1 p16/INK4a-CDK4/6-Rb-E2F1 pathway

INK4a plays an important role in G1/S cell cycle checkpoint regulation [33, 34]. It acts as an inhibitor of the cyclin D-dependent kinases, CDK4 and CDK6, by exclusively binding to them and preventing the formation of functional CDK 4, 6/cyclin D complexes [34]. INK4a is highly expressed in senescent cells in response to various stress situations [24, 35]. RAS can induce the expression of INK4a via MEK/MAPK pathway, and the accumulation of INK4a results in the inhibition of the kinase activity of CDK4/6, targeting on the retinoblastoma protein (Rb) [36, 37]. Hypophosphorylated Rb in turn recruitments the transcription factor E2F1 and form Rb/E2F1 complexes, blocking E2F1 from activating the transcription of different cell cycle-related genes, which may lead to cell cycle arrest and RAS-induced cellular senescence in vivo [38, 39]. It has been shown that the transcription of *Bmal1* can be activated by E2F1 [40], suggesting a potential role of CDK 4, 6/cyclin D-Rb-E2F1 pathway in regulating core circadian clock.

The complex formed by PER proteins, a class of core-clock factors, together with the multifunctional nuclear protein NONO, was found to bind to the promoter region of *Ink4a* with the help of unknown factors in a circadian pattern, leading to the transcriptional activation of *Ink4a* [41]. The circadian clock is coupled to cellular senescence via the inductive effect of PER/NONO complex on *Ink4a* transcription. A correlation between the transcriptional activity of PER2 protein and the expression of *Ink4a* mRNA have also been shown by Storcelova [42], which indicates that PER is a positive regulator of *Ink4a* and might be responsible for its circadian expression.

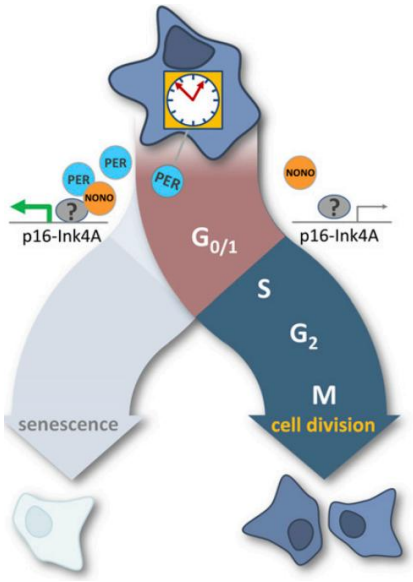

Figure 5: The PER/NONO complex regulates cellular senescence by activating the transcription of *Ink4a* [43]. The multifunctional nuclear protein NONO form a complex with PER in a circadian pattern and active the transcription of *Ink4a* by indirectly binding to its promoter region.

1.4.2.2 ARF-MDM2-p53 pathway

Numerous evidences suggest that ARF, another protein encoded by the CDKN2A locus, is also involved in cell cycle regulation, tumor pathogenesis and it plays an important role in p53 stabilization in stress- or oncogene-induced senescence [44-46]. The p53 tumor suppressor activates the transcription of MDM2, an E3 ubiquitin-protein ligase which can physically bind to p53 and induce p53 degradation, forming a negative feedback loop [47]. The accumulation of ARF activates p53 by sequestering MDM2, thereby inhibiting the MDM2-mediated proteolytic degradation of p53 [48]. It has been shown that p53 directly modulates the expression of *Per2* by binding to a response element in its promoter, which is overlapping with the E-box *cis*-element essential for the CLOCK/BMAL1 binding and the transcriptional activation of *Per2* [49]. The expression of ARF can be induced by MYC, which in turn is negatively regulated by the CLOCK/BMAL1 complex [27, 50].

1.4.3 p21/Cip1 interconnects p53 and Rb

p21/Cip1 (hereafter referred to as p21), encoded by the CDKN1A gene, is another cyclin-dependent kinase inhibitor, which competes with cyclin E for binding to Cdk2. The role of p21 in p53-induced cell cycle arrest and senescence is well characterized and p21 intermediates the crosstalk between INK4a-CDK4/6-Rb-E2F1 and ARF-MDM2-p53 pathways [51]. p53 actives the transcription of p21 in response to cellular stresses, such as oncogene overexpression and DNA damage [52]. Increased p21 inhibits the formation of CDK2/cyclin E complex, which then represses E2F1 activity via the CDK-Rb-E2F1 pathway [53, 54]. Contrary to INK4a, whose activity increases gradually after senescence-inducing stimuli, the level p21 is induced immediately upon the presence of stimuli and then decreases after a few day [55]. This points to a role of p21 in initiating the senescence response while INK4a acts to maintain this state.

1.5 Existing mathematical models of the mammalian circadian clock

Mathematical models have been of great help to gain a quantitative understanding of the crucial pathways and interactions in mammalian circadian clock regulation. Two common approaches used in modeling circadian clock are ordinary differential equations (ODEs) and delayed differential equations (DDEs). ODEs characterize details of the kinetics processes involved in the model, describing gene expression changes over time [56-58]. In case of poorly-characterized intermediary processes, such as post-translational modification and nuclear localization, DDEs introduce explicit time delays to reflect the fact that the action of a protein is delayed with respect to the time it is produced, serving in overcoming the missing information [59, 60].

One of the first basic models to describe the emergence of oscillations in negative feedback loops is the three-variable Goodwin oscillator with specific production and degradation rates [61, 62]. Several kinetic models of the mammalian circadian clock have been developed based on the three-component Goodwin oscillator. Although all of these models can produce sustained rhythms with approximately 24-hours periodicity, they are deficient in some respects: early models do not include all essential molecular components such as the nuclear receptor ROR and post-transcriptional modifications [56, 57], while other models are rather complex, making the estimation of kinetic parameters extremely difficult.

A single cell model for the mammalian clock containing the most essential biologically relevant processes but with intermediate complexity has been proposed by our group [9]. For simplicity, one gene family was represented by one variable in this model: *Per (Per1,2,3), Cry (Cry1,2), Ror (Rora,b,c), Rev-Erb (RevErbα,β) and Bmal (Bmal1,2)*. The mRNA, cytoplasmic protein and nuclear protein were distinguished for each gene entity, the nuclear shuttling and accumulation were modeled using nuclear import/export rates (Figure 6). The reversible phosphorylation/dephosphorylation process of PER proteins was also included in the model. CRYs associate with both hypophosphorylated and hyperphosphorylated PERs (PER*) in the cytoplasm. The PER/CRY and PER*/CRY complexes converge into PER/CRY_{pool} and repress the CLOCK/BMAL mediated transcription regulations. This model allows to study the PC loop and RBR loop independently, describing the mRNA and protein levels of the 5 core-clock genes over time. It is comprised of 19 ODEs with 71 parameters, which were obtained from the literature or estimated based on known phases and amplitudes using linear time-invariant (LTI) systems theory [63].

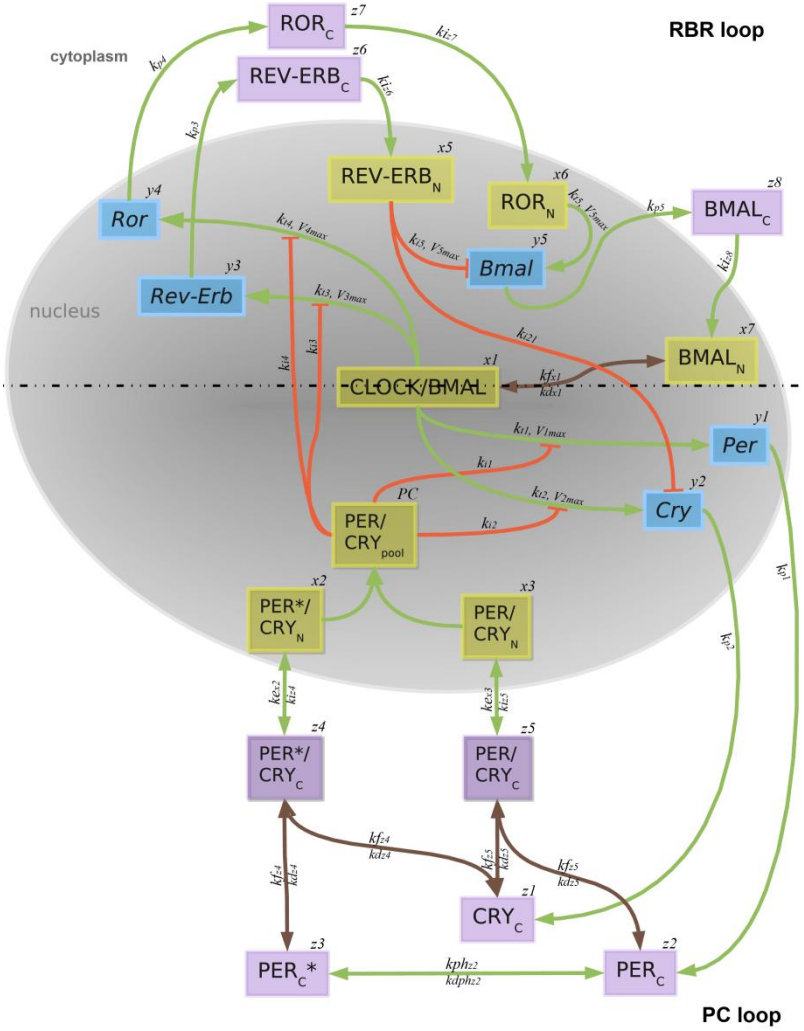

Figure 6: Model of the mammalian circadian clock [9]. This model contains two negative feedback loops: the PERs/CRYs (PC) loop and the RORs/Bmal/REV-ERBs (RBR) loop. For each gene entity, the mRNA (blue), cytoplasmic protein (purple) and nuclear protein (yellow) are distinguished. The transcriptional activation, translation, nuclear import/export, phosphorylation/dephosphorylation processes are represented using green lines, the transcriptional repressions are represented by red lines and complex formation/dissociation processes are represented using brown lines.

1.6 Aims

In the present project, we extended this previously developed mathematical model for the mammalian core-clock to include 25 additional ODEs and 96 additional parameters to simulate the interactions with the genes *Myc, Wee1*, and INK4a-CDK/CycD-Rb-E2F, ARF-MDM2-p53 pathways, which are involved in oncogene induced senescence. The extended network maintained the robust circadian oscillations of the system with a period of 23.65 hours and it achieved the optimal relative phase relations between the core-clock components. The comprehensive analysis of the newly extended model was used to interpret the experimental results produced in a mouse embryonic fibroblast (MEF) system. In this sytstem, INK4a/ARF$^{-/-}$ MEFs show different circadian clock phenotypes compared to wild-type (WT) MEFs upon RAS overexpression, suggesting that INK4a and

ARF may play crucial roles in Ras-induced effect on the circadian system. In addition, the model predictions of mRNA expression levels of core-clock genes upon different perturbations have been compared and validated by microarray data sets. The overall pipeline of the model construction and analysis is shown in Figure 7. We expect, with our results, to be able to provide a deeper insight into the dynamics of the cross-talk among the circadian system, oncogene induced proliferation/senescence and cancer.

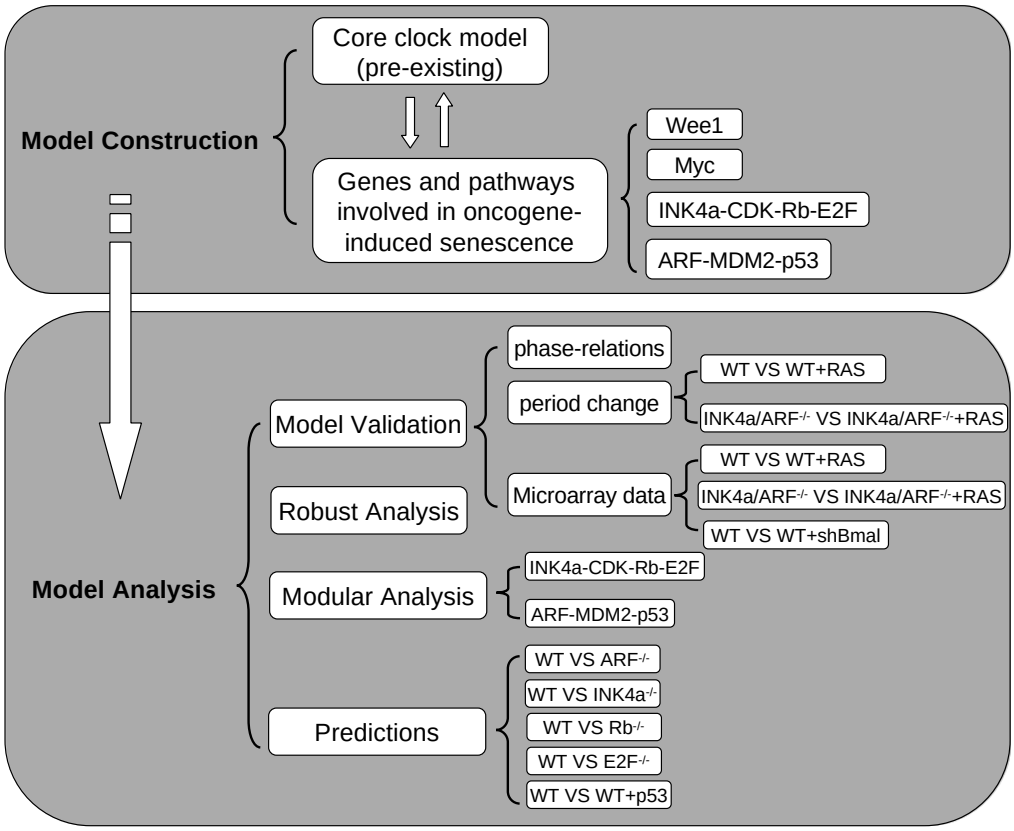

Figure 7: Project outline. The mathematical model for the mammalian core-clock was extended to genes and pathways involved in oncogene-induced senescence. The extended model was validated by essential features of the core circadian clock, experimental analysis of circadian phenotype in wild-type and INK4a/ARF$^{-/-}$ MEFs, and microarray data. The roles of INK4a-CDK-Rb-E2F pathway and ARF-MDM2-p53 pathway in RAS-induced period phenotype were analyzed independently. A series of predictions of circadian phenotype under different conditions were made with the extended model.

2. Materials and methods

2.1 Modeling data

The interactions between circadian clock and oncogene induced senescence were modeled by 25 ODEs and implemented using Matlab R2013a (Mathworks, Cambridge, UK), with ODE45, a build-in function for solving non-stiff differential equations using a Runge-Kutta method. Both of the relative error tolerance and the components of the absolute error tolerance vector were set to 10^{-9}. An integration step of 0.01 was used.

The transcriptional regulations were mathematically described using modified Hill-type kinetics, and the phosphorylation/dephosphoryplation processes were modeled by Michaelis-Menten type of kinetics. Complex formation/dissociation reactions, translation, import/export processes were modeled following the mass action law.

2.1.1 Mass action law

The mass action law describes the behaviors of a chemical reaction system when it reaches a state of dynamic equilibrium. According to the mass action law, the rate of an elementary chemical reaction is proportional to the concentrations of the reactants. For example, if

$$A+B \underset{k_r}{\overset{k_f}{\rightleftharpoons}} C$$

then the rate of change of reactants and product over time t can be defined as a set of ODEs:

$$\frac{d[A]}{dt} = k_r[C] - k_f[A][B] \quad (1)$$

$$\frac{d[B]}{dt} = k_r[C] - k_f[A][B] \quad (2)$$

$$\frac{d[C]}{dt} = k_f[A][B] - k_r[C] \quad (3)$$

2.1.2 Michaelis-Menten kinetics and Hill kinetics

Michaelis-Menten equation is one of the most commonly used model for enzymatic reactions. In this mechanism, it is assumed that the enzyme is not consumed and the total concentration of the enzyme ($[E]_0$) stays constant. The enzyme binds directly with the substrate to form an enzyme-substrate complex, which leads to the synthesis of the product [37]:

$$E+S \underset{k_r}{\overset{k_f}{\rightleftharpoons}} ES \xrightarrow{k_{cat}} E+P$$

Under the assumption that the substrate is in excess and ES is at a quasi-steady-state, which means

$$\frac{d[ES]}{dt} = k_f[E][S] - k_r[ES] - k_{cat}[ES] \approx 0 \quad (4)$$

Since $[E]_0 = [ES] + [E]$, then

$$[ES] = \frac{[E]_0[S]}{[S] + K_M} \tag{5}$$

where $K_M = \frac{k_r + k_{cat}}{k_f}$ is the Michaelis-Menten constant.

Based on mass action law, the rate of product formation can be described by:

$$\frac{d[P]}{dt} = k_{cat}[ES] = k_{cat}[E]_0 \frac{[S]}{K_M + [S]} = V_{max} \frac{[S]}{K_M + [S]} \tag{6}$$

where $V_{max} = k_{cat}[E]_0$ is the maximum reaction rate, obtained when all the enzyme binds to substrate. The Michaelis-Menten constant is the substrate concentration at which the reaction rate is half of V_{max}.

The Hill equation is an extension of the Michaelis-Menten kinetics. It is often written as

$$\frac{d[P]}{dt} = V_{max} \frac{[S]^n}{K_M^n + [S]^n} = V_{max} \frac{([S]/K_M)^n}{1 + ([S]/K_M)^n} \tag{7}$$

where n is the Hill coefficient, determining the degree of cooperativeness of the enzyme binding to the substrate or an ligand binding to the receptor. For non-cooperative binding, n equals to 1 and Hill kinetics is the same as the Michaelis-Menten kinetics.

2.1.3 Modeling of transcriptional regulation

In transcriptional regulation, an activator or a repressor can bind to multiple sites in the promoter region of the target gene, and/or the regulate may act as a multimer. It is common to use Hill-type kinetics to formulate the transcriptional regulation.

The transcriptional activation can be described as:

$$nA + G \underset{k_2}{\overset{k_1}{\rightleftharpoons}} A^nG$$

$$A^nG \xrightarrow{k_3} mRNA + A^nG$$

where A is the activator, G is the target gene and the mRNA is produced when A is bound to G.

It can be assumed that G exists as a single copy within a cell, i.e. $[G] + [AG] = 1$.

Since

$$\frac{d[A]^n}{dt} = k_1[A]^n[G] - k_2[A^nG] \approx 0 \tag{8}$$

Then the production of target mRNA is

$$\frac{d[mRNA]}{dt} = k_3[A^n G] = k_3 \frac{([A]/k_t)^n}{1 + ([A]/k_t)^n} = V_{max} \frac{([A]/k_t)^n}{1 + ([A]/k_t)^n} \tag{9}$$

where we call k_t the activation rate and $k_t^n = k_2/k_1$; $V_{max} = k_3$ is the transcription rate.

The transcriptional repression can be described as:

$$nR + G \underset{k_2}{\overset{k_1}{\rightleftharpoons}} R^nG$$

$$G \xrightarrow{k_3} mRNA + G$$

where R is the activator, G is the target gene and the mRNA is produced when R is not bound to G.

Similarly, the production rate of target mRNA is

$$\frac{d[mRNA]}{dt} = k_3[G] = k_3 \frac{1}{1 + ([R]/k_i)^n} = V_{max} \frac{1}{1 + ([R]/k_i)^n} \tag{10}$$

where k_i is the repression rate and $k_i^n = k_2/k_1$; $V_{max} = k_3$ is the transcription rate.

In our system, a modified Hill-type formalism with a new constant indicating the transcription fold activation was used to model the transcriptional activation, the production rate of the target mRNA can be described as:

$$\beta = V_{max} \frac{1 + a([A]/k_t)^n}{1 + ([A]/k_t)^n}, \quad a > 1 \tag{11}$$

All components in our system are subject to degradation, so that the rate of change of the target mRNA concentration is

$$\frac{d[mRNA]}{dt} = V_{max} \frac{1 + a([A]/k_t)^n}{1 + ([A]/k_t)^n} - d_{mRNA} mRNA, \quad a > 1 \tag{12}$$

where V_{max} and k_t are the transcription rate and activation rate parameters, respectively. a is the transcription fold activation, n is hill coefficient and d_{mRNA} is the degradation rate.

Similarly, in the transcriptional repression process, the rate of change of the target mRNA concentration is

$$\frac{d[mRNA]}{dt} = V_{max} \frac{1}{1 + ([R]/k_i)^n} - d_{mRNA} mRNA \tag{13}$$

2.2 Experiment data

2.2.1 Cell culture

Mouse embryonic fibroblasts (MEFs) from Wild-type (WT) and INK4a/ARF$^{-/-}$ knockout mice were cultured in Dulbecco's Modified Eagle Medium (DMEM, Gibco) supplemented with 10% fetal bovine serum (FBS), 1% Penicillin/Streptomycin and 25mM Hepes. Stable-transduced cells were selected with medium containing puromycin and hygromycin (Sigma). For live-cell bioluminescence measurement and analysis, cells were kept in phenol-red-free DMEM (Gibco) supplemented with 10% FBS, 1% penicillin/steptomycin and 0.1 mM D-Luciferin (PJK). Optical microscopy was used to check cell morphology and density. All cultures were incubated at 37°C with 5% CO_2 atmosphere.

2.2.2 Lentivirus production

HEK293T cells were seeded in 175 cm^2 angled neck culture flasks and cotransfected with 12.5 µg packaging plasmid psPAX, 7.5µg envelope plasmid pMD2G and 17.5µg BMAL1-promoter (BLP) luciferase expression plasmid using the CalPhos mammalian transfection kit (Clontech) following the manufacturer's protocol. To harvest lentiviral particles, cell debris was removed by centrifugation at 4100×g for 15 min and the lentivirus-containing supernatant was passed through a 45µm filter. The obtained lentivirus was stored at -80°C.

2.2.3 Lentiviral transduction

All cells were seeded in 35mm dishes (1ml of cell suspension) and 1ml lentiviral supernatant containing 8µg/ml protamin sulphate (Sigma-Aldrich) was added. Cells were incubated with Bmal1-promoter luciferase reporter overnight at standard cell culture conditions. Medium was removed and selection medium (DMEM supplemented with 10% FBS, 1% penicillin/streptomycin) containing puromycin (10µg/ml) or hygromycin (100µg/ml) was added and changed every third day. Cells were cultured until they reached 80% of confluency.

To overexpress H-Ras in MEFs, low passage Phoenix cells were grown in a 10 cm^2 petri-dish to a maximal density of 70%. 20 µg MSCV-Ras-BSD plasmid, 15 µg helper plasmid and 62.5 µl $CaCl_2$ were mixed in a FACS tube and adjusted with sterile water to 500 µl. After adding 500 µl 2 x HBS dropwise under constant agitation (air bubbles), DNA precipitation occurred within 5 minutes at RT (mixture gets milky and cloudy). Meanwhile, old medium of Phoenix cells was exchanged. Subsequently, 10 ml DMEM medium containing 25 µM chloroquine and the precipitate (1 ml) were added. After 12 hours incubation, medium including the precipitate was replaced by 5 ml of DMEM medium for collecting virus supernatant.

MEF cells that were about to be infected were seeded at subconfluent density 12 hours after Phoenix cell transfection. The first virus supernatant was harvested within 12 hours after transfection by aspiration and filtered through a 0.45 µm filter. Medium was removed from the cells and virus supernatant including 4 µg/ml polybrene was added. New medium was added to the Phoenix cells for the next round of infection. Afterwards, cells were incubated and grown under standard conditions.

After 12 hours of incubation, the second virus supernatant was harvested according to the procedure above, supplemented with polybrene and added. After spinoculation of the plates (1500 rpm, 10 minutes, 32°C), cells were incubated and grown until the next round of transduction. In addition, new medium was added to the Phoenix cells for the next round of transduction. The third and fourth virus supernatants were collected 12 hours and 24 hours later according to the procedure above.

12 hours after the last transduction, medium was removed from the cells and fresh DMEM medium containing 10 µg/ml blasticidin was added. Cells were selected for 3 days. Medium was changed and the cells were cultivated for 5 days to be taken for further experiments.

2.2.4 Adriamycin treatment

MEF cells were seeded at subconfluent density in 6 well plate and incubated for 12 hours until all the cells were attached to the plate. Adriamycin was added to the medium to the final concentration of 0.01 mg/ml. Medium was changed after 3 days and cells were cultivated for 2 more days and harvested for further experiments.

2.2.5 Synchronization and measurement of circadian rhythms

Each cell type in culture was specifically tested both prior to the live-cell bioluminescence recording and posterior to transduction with the lentivirus harbouring the BMAL1-Luciferase reporter to make sure that confluency is reached only by the end of the measurements. To measure rhythmic bioluminescence, transduced cells were synchronized with a single pulse of 1mM dexamethasone (Sigma) for 45 minutes. After washing once with 1xPBS, the cells were cultured in phenol-red-free DMEM containing 0.1 mM D-Luciferin. Luciferase activity was measured by LumiCycle (Actimetrics) with a photomultiplier tube (PMT)-based system (Hamamatsu Photonics).

2.2.6 Circadian data

Periods, phases and amplitudes were estimated by fitting the cosine wave function using the ChronoStar analysis software [64]. Data were smoothed by taking a 4 hours-running average for visualization. Basal luciferase levels from raw data were included by the fold change in luciferase activity relative to GFP controls for de-trended and smoothed data.

3. Results

3.1 Experimental data

To study the molecular mechanisms underlying the interactions between circadian clock and cellular senescence versus proliferation, our group used a well-controlled cell culture system, which compared morphological phenotypes of wild-type and INK4a/ARF-knockout MEFs upon transient induction of H-RAS and suggested a prominent role of the CDKN2A locus in mediating RAS-induced senescence [65, 66]. From Figure 8A-D, it can be observed that normal MEFs undergo senescence while their INK4a/ARF-deficient counterparts undergo accelerated proliferation when H-RAS was lentivirally over-expressed, which is in agreement with previous studies. In order to analyze the circadian phenotypes, MEFs were lentivirally transduced with a reporter vector in which the luciferase activity is regulated by the promoter of *Bmal1* to monitor its oscillation dynamics. From the bioluminescence measurements, we observed that circadian periods of wild-type and INK4a/ARF$^{-/-}$ MEFs were similar: 24.11 and 24.28 hours respectively. However, wild-type MEFs exhibited an increased period of T = 26.61 hours, whereas the INK4a/ARF$^{-/-}$ MEFs showed an decreased period of T = 23.89 hours upon RAS overexpression (Figure 8E-H). Several repeated trails have been carried out in our group and confirmed this observation. These data suggested that INK4a and ARF, the key mediators of RAS-induced senescence are also involved in the circadian clock deregulation upon RAS induction.

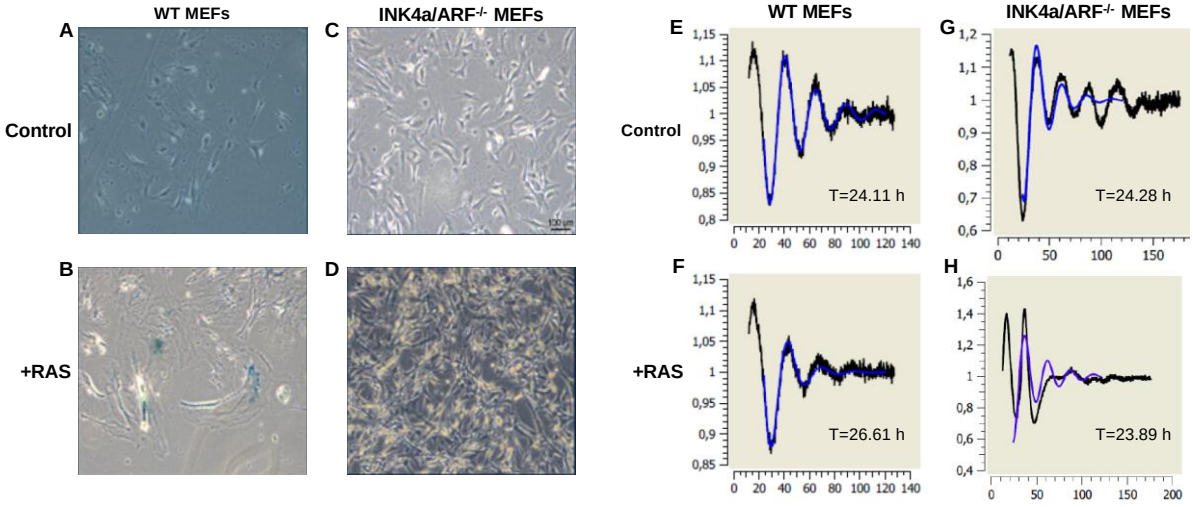

Figure 8: WT and INK4a/ARF$^{-/-}$ MEFs shows opposite morphological phenotypes and circadian phenotypes (unpublished data, manuscript in preparation). (**A-D**) β-Gal staining of WT MEFs and INK4a/ARF$^{-/-}$ MEFs upon the induction of H-RAS (**B, D**) and their corresponding control (**A, C**). (**E-H**) Analysis of circadian period in WT MEFs and INK4a/ARF$^{-/-}$ MEFs upon H-RAS overexpression (**F, H**) and their corresponding control (**E, G**). The black line is the trendeliminated data and the blue line is the fit by ChronoStar analysis software.

3.2 Model design

To investigate the underlying mechanisms of RAS-induced effect on the circadian clock in a proliferation vs senescence scenario, we extended our previous developed mathematical model of the core circadian clock to external genes, *Myc* and *Wee1*, and signaling pathways, INK4a-CDK4/6-Rb-E2F1 pathway and ARF-MDM2-p53 pathway, which are involved in oncogene-induced senescence. The newly extended model uses ODEs to describe the dynamics and kinetics of the system, it consists of 45 variables and 167 parameters in total, out of which 20 variables and 71 parameters were directly adapted from the previously-built mathematical model for mammalian circadian clock (hereafter referred to as "original model") [9]. The transcriptional regulations were modeled based on Hill-type kinetics (Section 2.1.3), the translation, complex formation/dissociation, nuclear import processes were modeled according to Mass action law (Section 2.1.1) and Michaelis-Menten kinetics were used to model protein phorsphorylation/dephorsphorylation processes (Section 2.1.2). For simplicity, we assumed that the new protein components in the model were unidirectionally translocate to nucleus, the nuclear export process could be reflected in the nuclear import rates.

Extensive literature search has been done to estimate newly added parameters. Most of the degradation rates and some Michaelis-Menten constants, phosphorylation/dephosphorylation rates, protein complex formation/dissociation rates were retrieved from the literature. For the remaining free parameters, the average value of the same type of parameters in the pre-existing core-clock model was used, additionally some of them were fine-tuned to fit our experimental observations. Robustness analysis has been performed by introducing +/- 10% perturbation to each parameter and the model was robust to those changes (Appendices Table S3). Figure 9 shows a simplified schematic diagram of the model, and a more detailed view of the system is provided in Figure 10. It should be noted that some links shown in the figures are indirect interactions, the corresponding references for each link are given in Figure S1 (Appendices). The list of variables is given in Table S1 (Appendices), parameters and their values are shown in Table S2 (Appendices). In this section, I will explain how the extended model is built based on biological facts step by step.

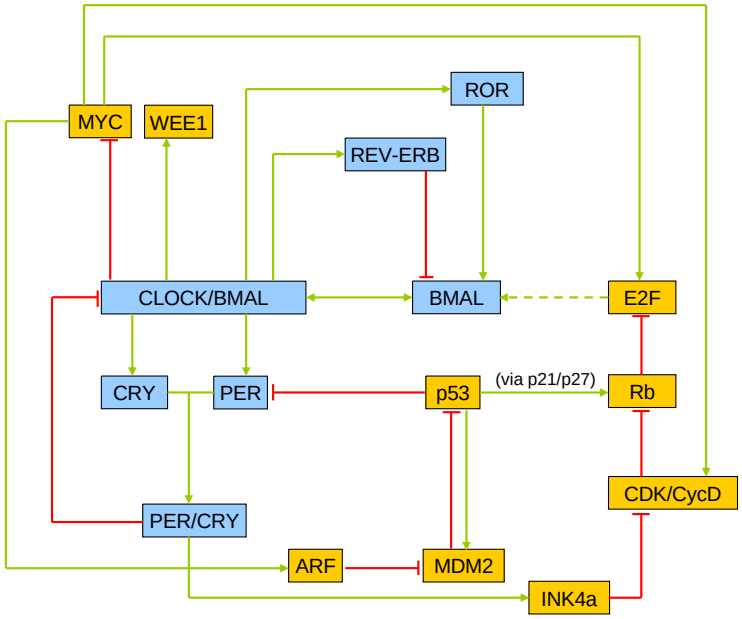

Figure 9: Simplified schematic diagram of the extended network. The species in blue boxes are components (including genes and proteins) already included in the pre-exsiting mathematical model for mammalian core circadian clock and the species in yellow boxes are newly added components in the extended model. Green arrows represents transcriptional activation and complex formation/dissociation processes, the green dashed arrow indicates potential transcriptional activation reported in a database (MotifMap); and red lines represents inhibitory effects, including transcriptional repression and physical protein-protein association.

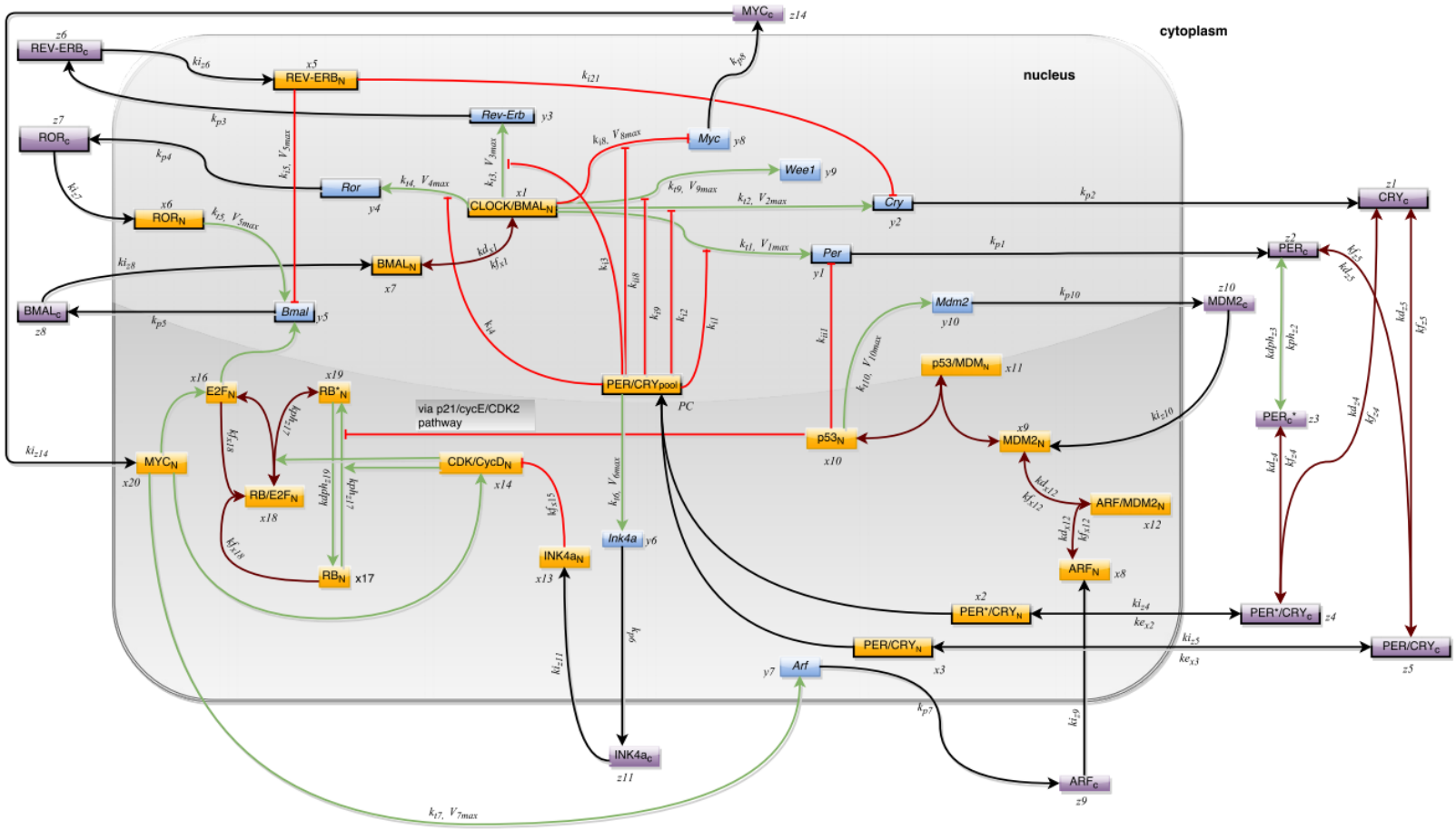

Figure 10: Detailed diagram of the extended network. The network comprises two compartments: the nucleus and the cytoplasm (as marked in the figure). There are 45 variables including 14 genes in total, out of which 20 variables (boxes with black border) including 5 genes are adapted from our pre-existing mathematical model for core circadian clock. For each gene entity, the mRNA (blue), cytoplasmic protein (purple) and nuclear protein (yellow) are distinguished. The transcriptional activation, phosphorylation/dephosphorylation processes are represented using green lines, the transcriptional repressions are represented by red lines. Translation and nuclear importation/exportation processes are represented by black lines while complex formation/dissociation processes are represented using brown lines.

3.2.1 Extend the model to *Wee1*, *Myc*, *Ink4a* and *Arf*

The CLOCK/BMAL complex can regulate the expression of cell cycle checkpoint genes, *Wee1* and *Myc*, by directly binding to the E-box *cis*-element in their promoter region [31, 32]. The binding of CLOCK/BMAL activates the transcription of *Wee1* while it repress *Myc* transcription. Following the principle in the original model, the PER/CRY_{pool} including all possible PER/CRY heterodimers has an inhibitory effect on the CLOCK/BMAL mediated transcriptional regulations (Figure 11). As mentioned above, the mRNA, cytoplasmic protein and nuclear protein are modeled independently for each element in this system.

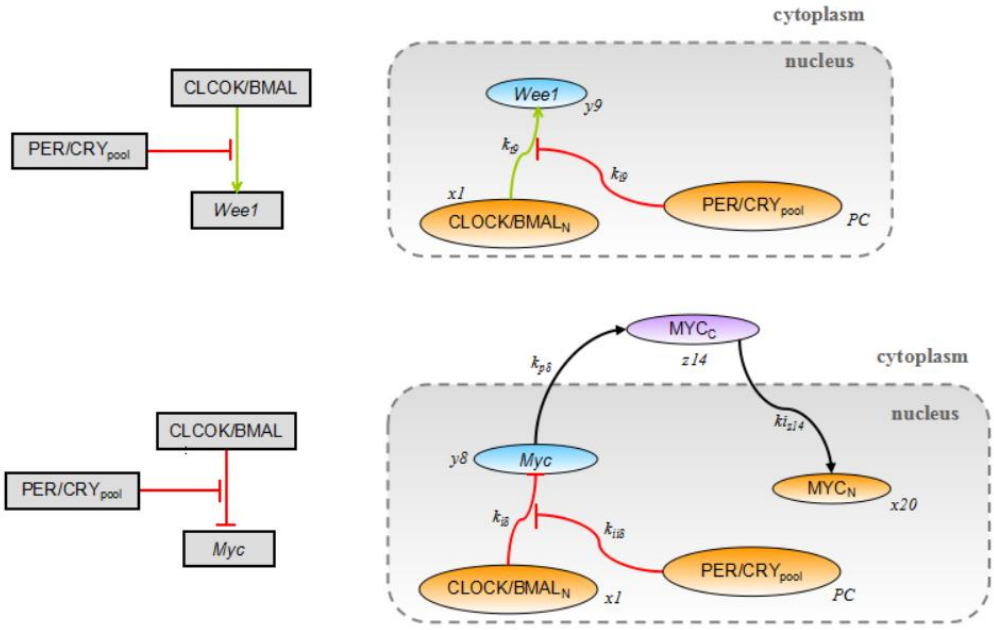

Figure 11: *Wee1* and *Myc* are regulated by core-clock genes. The transcription of *Wee1* and *Myc* is activated and inhibited by the CLOCK/BMAL complex, respectively and these regulations are repressed by PER/CRY heterodimers. Green arrow represents transcriptional activation; red lines represent transcriptional repression processes; translation and nuclear import processes are represented by black arrows.

The corresponding ODEs for *Wee1* and *Myc* are given as following:

Wee1

$$\frac{dy9}{dt} = V_{9max}\frac{1 + l1\left(\frac{x1}{k_{t9}}\right)^{h6}}{1 + \left(\frac{x1}{k_{t9}}\right)^{h6} + \left(\frac{PC}{k_{i9}}\right)^{h7}\left(\frac{x1}{k_{t9}}\right)^{h6}} - d_{y9}y9 \quad (14)$$

Myc

$$\frac{dy8}{dt} = V_{8max}\frac{1}{1 + \frac{k_{ii8}^{h5}}{k_{ii8}^{h5} + PC^{h5}}\left(\frac{x1}{k_{i8}}\right)^{h4}} - d_{y8}y8 \quad (15)$$

MYC_c $$\frac{dz14}{dt} = k_{p8}(y8 + y8_0) - ki_{z14}z14 - d_{z14}z14 \quad (16)$$

MYC_N $$\frac{dx20}{dt} = ki_{z14}z14 - d_{x20}x20 \quad (17)$$

The PER proteins, together with the nuclear protein NONO, have been found to active the transcription of *Ink4a* by binding to its promoter in a circadian manner [41]. As the PER/CRY_{pool} is positively correlated with PER, the activator of *Ink4a*, it is reasonable to lump the series of interactions into the positive correlation between PER/CRY_{pool} and *Ink4a* transcription without losing essential dynamic features of the system. The INK4a protein, which is known as a potent inhibitor of D-type cyclin-dependent kinases, compete for binding to CDK4/6 with CycD and inhibit the subsequent Rb phorsphorylation. In this model we use CDK to represent all CDKs inhibited by INK4a, namely CDK4 and CDK6.

Evidence showed that the expression of ARF, the other product encoded by the CDKN2A locus, can be induced by MYC [50]. Even though it is not clear if the inductive effect is achieved through directly binding to the promoter of *Arf* gene, it is common to model the interaction using hill-type kinetics [67]. Accumulated ARF stabilizes p53 by binding to MDM2, a E3 ubiquitin ligase targeting on p53 in the nucleus [48].

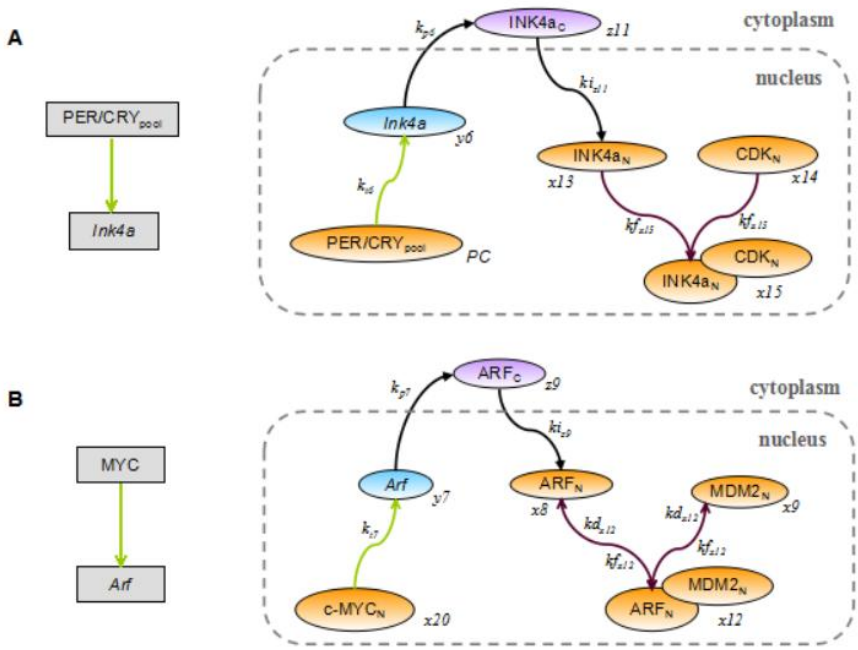

Figure 12: Detailed diagram of reactions involving *Ink4a* and *Arf*. Green arrow represents transcriptional activation; red lines represent transcriptional repression processes; brown arrows represent complex formation/dissociation processes; translation and nuclear import processes are represented by black arrows.

The ODEs describing the dynamics of INK4a and ARF are given as following, the equations for CDK and MDM2 are given in Section 3.2.2 and 3.2.3 respectively.

Ink4a

$$\frac{dy6}{dt} = V_{6max}\frac{1 + o\left(\frac{PC}{k_{t6}}\right)^{r}}{1 + \left(\frac{PC}{k_{t6}}\right)^{r}} - d_{y6}y6 \tag{18}$$

$INK4a_c$

$$\frac{dz11}{dt} = k_{p6}(y6 + y6_0) - ki_{z11}z11 - d_{z11}z11 \tag{19}$$

$INK4a_N$

$$\frac{dx13}{dt} = ki_{z11}z11 - kf_{x15}x13x14 - d_{x13}x13 \tag{20}$$

Arf

$$\frac{dy7}{dt} = V_{7max}\frac{1 + l\left(\frac{x20}{k_{t7}}\right)^{s}}{1 + \left(\frac{x20}{k_{t7}}\right)^{s}} - d_{y7}y7 \tag{21}$$

ARF_c

$$\frac{dz9}{dt} = k_{p7}(y7 + y7_0) - ki_{z9}z9 - d_{z9}z9 \tag{22}$$

ARF_N

$$\frac{dx8}{dt} = ki_{z9}z9 - kf_{x12}x8x9 - d_{x8}x8 \tag{23}$$

3.2.2 INK4a-CDK/CycD-Rb-E2F pathway and its regulation of *Bmal*

In order to interpret the circadian phenotype of INK4a/ARF-knockout MEFs, it is necessary to extend the model with a feedback from INK4a and ARF to the core circadian clock. Our first candidate is the INK4a- CDK/CycD-Rb-E2F pathway. On one hand, the transcription factor MYC directly induces the synthesis of *Cdk4* [68]. CDK4 and another cyclin D-dependent kinase CDK6 form active complex with CycD and play important roles in the phosphorylation of Rb, the key regulator of E2F family transcription factors. Once Rb is phosphorylated, active E2F will be released from the Rb/E2F complex [34, 38, 39]. It has been shown that E2F activators (E2F1, E2F2, and E2F3a) can potentially bind to the promoter of *Bmal1* and activate its transcription [40]. On the other hand, the formation of CDKs/CycD complex is inhibited by INK4a, which has a negative effect on Rb phosphorylation and reinforce the inhibition on E2F. MYC also promotes the transcription of the three E2F activators [69, 70]. In this model, we used E2F to represent the three activators belonging to E2F family, i.e. E2F1, E2F2, and E2F3a.

In addition, the tumor suppressor protein p53 inhibits the phorsphorylation of Rb via p21/p27-CDK/CycE-Rb pathway. Both p21/Cip and p27/Kip are inhibitors of cyclin E-dependent kinase CDK2, which regulates Rb phosphorylation and E2F activity synergistically with CDK4/CycD and CDK6/CycD. The transcription of p21/Cip can be induced by p53. To reduce the complexity, the effect of the p53-p21/p27-CDK/CycE arm was lump into a negative correlation between p53 and the enzymatic activity of CDK/CycE.

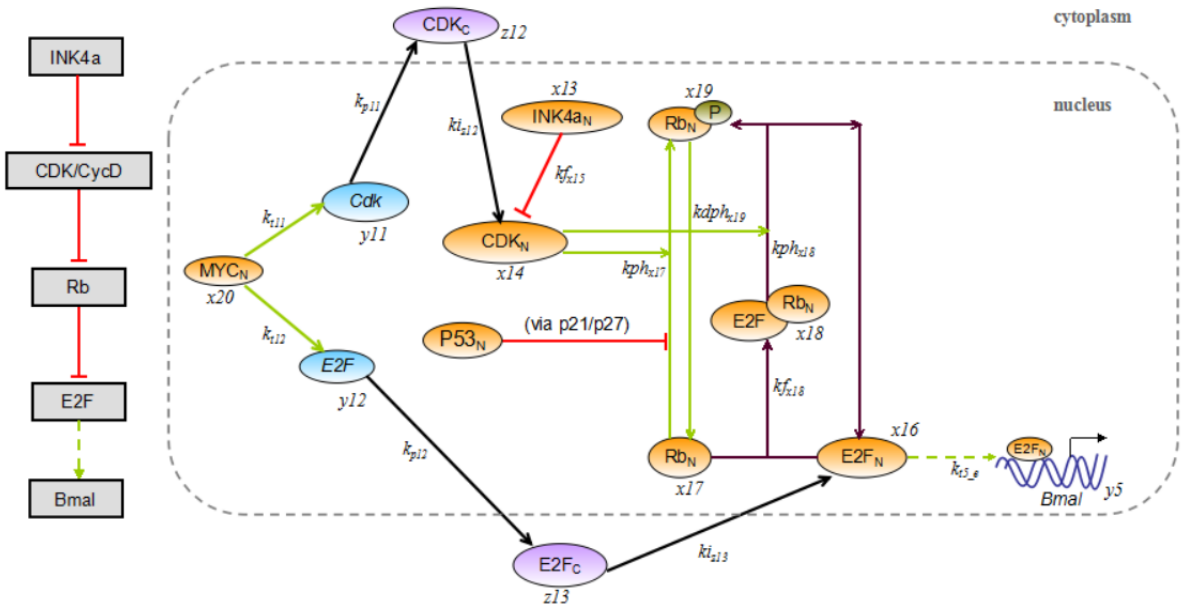

Figure 13: Detailed reaction diagram of INK4a-CDK/CycD-Rb-E2F pathway and its effect on *Bmal* transcription. Green arrow represents transcriptional activation and phosphorylation/dephosphorylation processes; red lines represent transcriptional repression processes; brown arrows represent complex formation/dissociation processes; translation and nuclear import processes are represented by black arrows.

The corresponding ODEs describing the molecular mechanisms of the INK4a-CDK/CycD-Rb-E2F pathway and the interactions between p53 and Rb are given as following:

Cdk

$$\frac{dy11}{dt} = V_{11max}\frac{1 + r2\left(\frac{x20}{k_{t11}}\right)^{h2}}{1 + \left(\frac{x20}{k_{t11}}\right)^{h2}} - d_{y11}y11 \quad (24)$$

CDK_c

$$\frac{dz12}{dt} = k_{p11}(y11 + y11_0) - ki_{z12}z12 - d_{z12}z12 \quad (25)$$

CDK_N

$$\frac{dx14}{dt} = ki_{z12}z12 - kf_{x15}x13x14 - d_{x14}x14 \quad (26)$$

E2F

$$\frac{dy12}{dt} = V_{12max}\frac{1 + r3\left(\frac{x20}{k_{t12}}\right)^{h3}}{1 + \left(\frac{x20}{k_{t12}}\right)^{h3}} - d_{y12}y12 \quad (27)$$

$E2F_c$

$$\frac{dz13}{dt} = k_{p12}(y12 + y12_0) - ki_{z13}z13 - d_{z13}z13 \quad (28)$$

$E2F_N$

$$\frac{dx16}{dt} = ki_{z13}z13 - kph_{x17}\left(x14 + \frac{Kbp}{Kbp + x10}\right)\frac{x18}{x18 + Kph} - kf_{x18}x16x17 - d_{x16}x16 \quad (29)$$

Rb_N

$$\frac{dx17}{dt} = source\_Rb + kdph_{x19}\frac{x19}{x19 + Kdph} - kph_{x17}\left(x14 + \frac{Kbp}{Kbp + x10}\right)\frac{x17}{x17 + Kph} - kf_{x18}x16x17 - d_{x17}x17 \quad (30)$$

E2F/Rb

$$\frac{dx18}{dt} = kf_{x18}x16x17 - kph_{x17}\left(x14 + \frac{Kbp}{Kbp + x10}\right)\frac{x18}{x18 + Kph} - d_{x18}x18 \quad (31)$$

Rb^*_N

$$\frac{dx19}{dt} = kph_{x17}\left(x14 + \frac{Kbp}{Kbp + x10}\right)\left(\frac{x17}{x17 + Kph} + \frac{x18}{x18 + Kph}\right) - kdph_{x19}\frac{x19}{x19 + Kdph} - d_{x19}x19 \quad (32)$$

In order to include the inductive effect of E2F on *Bmal1* transcription, which is not shown in the original model. The equation describing *Bmal* expression dynamics was changed from

$$\frac{dy5}{dt} = V_{5max}\frac{1 + i\left(\frac{x6}{k_{t5}}\right)^n}{1 + \left(\frac{x5}{k_{i5}}\right)^m + \left(\frac{x6}{k_{t5}}\right)^n} - d_{y5}y5 \quad (33)$$

in the original model to

$$\frac{dy5}{dt} = V_{5max}\frac{1 + i\left(\frac{x6}{k_{t5}}\right)^n}{1 + \left(\frac{x5}{k_{i5}}\right)^m + \left(\frac{x6}{k_{t5}}\right)^n}\frac{1 + a\_1\left(\frac{x16}{k_{t5\_e}}\right)^{a\_2}}{1 + \left(\frac{x16}{k_{t5\_e}}\right)^{a\_2}} - d_{y5}y5 \quad (34)$$

in the newly-extended model, where x16 is the variable representing E2F, and a_1, a_2, kt5_e are the corresponding transcription fold activation, hill coefficient, and activation rate, respectively.

3.2.3 ARF-MDM2-p53 pathway and its regulation of *Per*

The ARF-MDM2-p53-Per pathway is a feedback from the external gene ARF to the core circadian clock. As mentioned in Section 1.4.2 and Section 3.2.1, the expression of ARF can be activated by MYC. The accumulated ARF physically associates with MDM2 and leads to rapid degradation of MDM2, thereby inhibiting the MDM2-mediated degradation of p53 and promoting p53 stabilization and accumulation. Recent evidence showed that there is a p53 response element located in the promoter region of *Per2* gene and the response element overlaps with the E-box *cis*-element crucial for CLOCK/BMAL-mediated *Per2* transcription. The binding of p53 strongly represses the transcription of *Per2* by competing with CLOCK/BMAL for binding to the *Per2* promoter.

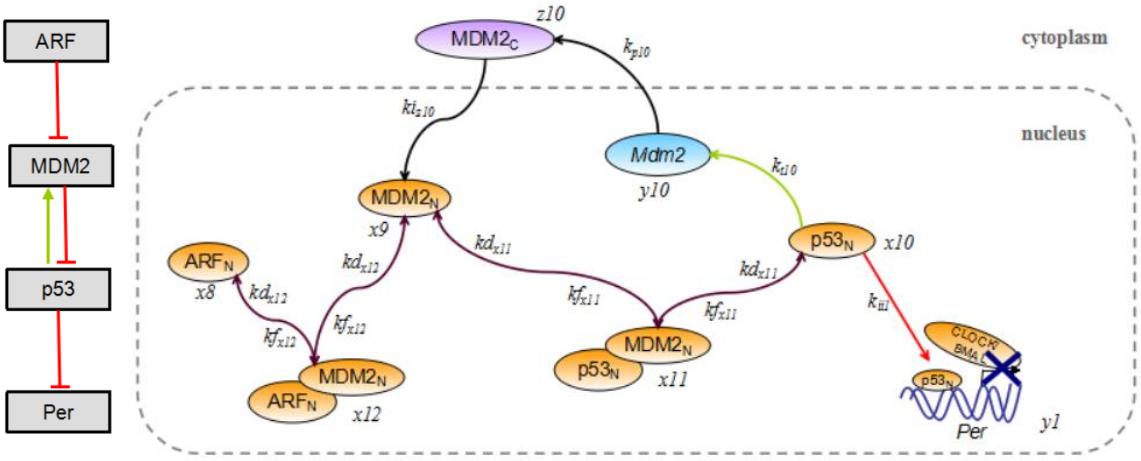

Figure 14: Detailed reaction diagram of ARF-MDM2-p53 pathway and its effect on CLOCK/BMAL-mediated transcription of *Per*. Green arrow represents transcriptional activation; red lines represent transcriptional repression processes; brown arrows represent complex formation/dissociation processes; translation and nuclear import processes are represented by black arrows.

The ODEs describing the dynamics of the elements involved in ARF-MDM2-p53 pathway are given as following:

Mdm2

$$\frac{dy10}{dt} = V_{10max}\frac{1 + r1\left(\frac{x10}{k_{t10}}\right)^{h1}}{1 + \left(\frac{x10}{k_{t10}}\right)^{h1}} - d_{y10}y10 \quad (35)$$

$MDM2_c$

$$\frac{dz10}{dt} = k_{p10}(y10 + y10_0) - ki_{z10}z10 - d_{z10}z10 \quad (36)$$

$MDM2_N$

$$\frac{dx9}{dt} = ki_{z10}z10 + kd_{x11}x11 + kd_{x12}x12 - kf_{x11}x9x10 - kf_{x12}x8x9 - d_{x9}x9 \quad (37)$$

$p53_N$

$$\frac{dx10}{dt} = source\_p53 + kd_{x11}x11 - kf_{x11}x9x10 - d_{x10}x10 \quad (38)$$

$MDM2/ARF_N$

$$\frac{dx12}{dt} = kf_{x12}x8x9 - kd_{x12}x12 - d_{x12}x12 \quad (39)$$

$MDM2/p53_N$

$$\frac{dx11}{dt} = kf_{x11}x9x10 - kd_{x11}x11 - d_{x11}x11 \quad (40)$$

In order to describe the repression of p53 on the expression of *Pers*, which is not shown in the original model, the equation describing *Per* expression dynamics was changed from

$$\frac{dy1}{dt} = V_{1max} \frac{1 + a\left(\frac{x1}{k_{t1}}\right)^{b}}{1 + \left(\frac{PC}{k_{i1}}\right)^{c}\left(\frac{x1}{k_{t1}}\right)^{b} + \left(\frac{x1}{k_{t1}}\right)^{b}} - d_{y1}y1 \quad (41)$$

in the original model to

$$\frac{dy1}{dt} = V_{1max} \frac{1 + a\left(\frac{x1}{k_{t1}}\right)^{b}}{1 + \left(\frac{PC}{k_{i1}}\right)^{c}\left(\frac{x1}{k_{t1}}\right)^{b} + \left(\frac{x1}{k_{t1}}\right)^{b} + \left(\frac{x10}{k_{ii1}}\right)^{h8}\left(\frac{x1}{k_{t1}}\right)^{b}} - d_{y1}y1 \quad (42)$$

in the newly-extended model, where $\left(\frac{x10}{k_{ii1}}\right)^{h8}\left(\frac{x1}{k_{t1}}\right)^{b}$ models the repression effect of p53 on *Per* transcription via competing for DNA binding with CLOCK/BMAL.

3.3 Model analysis

3.3.1 The extended model reproduces essential features of the core circadian system

To make sure that the extended model maintains the main biological features and does not disrupt the oscillations of the core circadian system, we tested the period, amplitudes and phases of the *in silico* mRNA expression patterns of core-clock genes, i.e. *Bmal, Per, Cry, Ror, Rev-Erb*, and also the cytoplasmic and nuclear PER/CRY protein complexes, including both phosphorylated and unphosphorylated species. All the expression levels were normalized to the corresponding average value. The period of the system was set to 23.65 hours by fine-tuning a scaling factor used in the model to adjust the period of the system. The phase of *Bmal* mRNA expression oscillations was manually set to 9 pm (21:00) which is exactly the same as that simulated in the original model [9].

The amplitude of the simulated oscillatory expression of *Bmal* mRNA generated by the extended model is higher in comparison with what was shown in the original model, we speculate this might due to the inductive effect of E2F on *Bmal*, which was not included in the original model (Figure 15). The decrease in the amplitude of *Per* mRNA is considered as a result of the transcriptional repression mediated by p53. It is worth noting that although a slight phase shift is observed in the simulated expression, each core-clock component peaks in the corresponding published time (Figure 16). Furthermore, the extended model also successfully achieves the proper phase relations among the core-clock components, which is essential for the network to generate proper oscillations. A comparison of the peaks of the simulated core-clock components expression between the original model and the extended model as well as the published optimal time intervals is shown in Figure 16, and the corresponding values are given in Table 1. These results indicate that the newly extended model can reproduce the essential features of the core circadian system and can be subsequently used to interpret the experimental data related to circadian phenotypes and make further predictions.

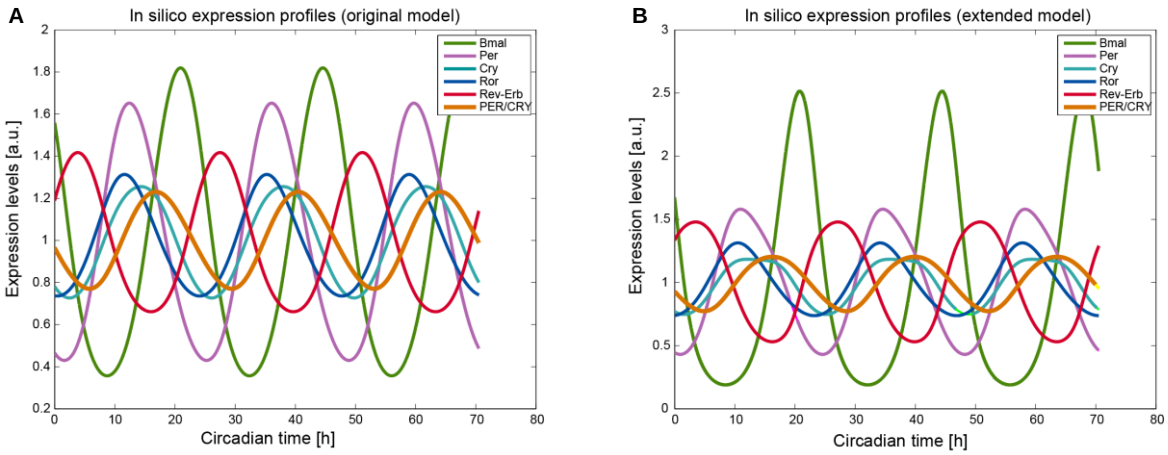

Figure 15: Comparison of *in silico* expression profiles of core-clock components obtained from the simulations with the original model and extended model. The period and the phase of *Bmal* expression in the extended system were set to 23.65 hours and 9 pm (21:00), respectively, which are exactly the same as in the original model. The phases-relations among the core-clock components achieved in the extended model are same as in the original model.

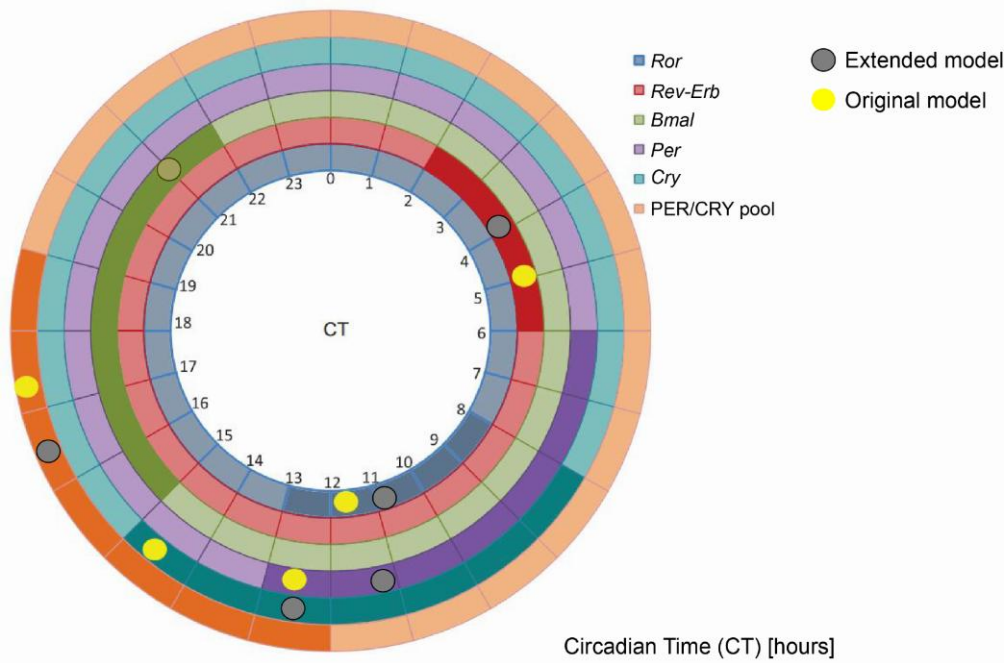

Figure 16: In *silico* phase data of the extended model fits with data of original model and with known experimental data. The original diagram is adapted from the original model [9]. The published time interval in which the mRNAs of *Ror* (blue) , *Rev-Erb* (red), *Bmal* (green), *Per* (purple), *Cry* (turquoise) and the cytoplasmic and nuclear PER/CRY protein complexes (PER/CRY_{pool}: orange) show highest expression are marked by relatively dark color. The full yellow circles represent the peak of expression simulated with the original model and the full grey circle represent the peak of expression simulated with the extended model.

Table 1: Comparison of peak phases data obtained from original and extended models. The corresponding published time intervals are given as reference.

Core-clock genes	Phase (CT) [hours]		Shift [hours]	Optimal time interval (CT) [hours]
	Original model	Extended model		
Bmal	21	21	0	15 - 22
Rev-Erb	3.96	3.8	0.16	2 - 6
Ror	11.75	10.97	0.78	8 - 13
Per	12.42	11.3	1.12	6 - 13
Cry	14.64	12.52	2.12	8 - 15
PC_{pool}	17.10	16.32	0.78	12 - 19

3.3.2 Simulation of experimental data with the extended model

As shown in Section 3.1, the experimental data from a well-established cell culture system showed that the WT and INK4a/ARF$^{-/-}$ MEFs exhibited different circadian phenotypes upon RAS perturbation: WT MEFs showed a longer period, whereas the INK4a/ARF$^{-/-}$ MEFs showed a shorter period in response to RAS overexpression. Published data shows that MAPK, a key downstream effector activated by RAS via Ras-Raf-MEK pathway, can directly interact with and phosphorylate BMAL1, leading to a negative effect on the CLOCK/BMAL-mediated transcriptional activation/repression [71]. In our model, we used the activation/inhibition rates (kt or ki) to characterize the transactivation/transrepression capacity. In order to model the effect of RAS overexpression, we adapted a method from the previous work on RAS-mediated deregulation of the circadian clock in cancer, in which a factor ktt was introduced to activation/inhibition rates in the terms describing CLOCK/BMAL mediated transcription: $ktt=1$ was used to describe a normal RAS expression and $ktt<1$ indicates a reduced transcriptional activation/repression capacity of CLOCK/BMAL caused by RAS overexpression [72]. For example, $ktt=0.6$ means that there is a 40% reduction in CLOCK/BMAL mediated transcription.

Besides repressing CLOCK/BMAL-mediated transcriptional regulation, RAS can also induce the expression of INK4a via MEK/MAPK pathway [36], we used a term depending on ktt to model the inductive effect of RAS on *Ink4a* transcription, without introducing extra parameters:

Ink4a
$$\frac{dy6}{dt} = (1 + ln\frac{1}{ktt})V_{6max}\frac{1 + o\left(\frac{PC}{k_{t6}}\right)^r}{1 + \left(\frac{PC}{k_{t6}}\right)^r} - d_{y6}y6 \qquad (43)$$

When RAS is normal expressed, ktt is set to 1, and the term $1 + ln\frac{1}{ktt}$ equals to 1, which means *Ink4a* is also normally expressed. When RAS is over-expressed, ktt is set to a value lower than 1 and $1 + ln\frac{1}{ktt}$ gains a value larger than 1, indicating that the production rate of *Ink4a* mRNA is increased. It need to be noted that the system is subject to $0<ktt<e$ to make sure that the production rate of *Ink4a* mRNA is positive.

The *in silico Ink4a* expression profiles in WT MEFs (Figure 18) shows that the expression level of *Ink4a* when $ktt=0.6$ (i.e. RAS overexpression resulting in a 40% reduction in the transcriptional

activation/repression capacity of CLOCK/BMAL) is much higher than that when $ktt=1$ (under normal condition), which is in agreement with published experimental data [36].

The condition of INK4a/ARF-knockout was modeled by setting the initial conditions of the mRNAs, cyctoplasmic proteins and nuclear proteins of both INK4a and ARF to 0, and the rate of change of their concentration were also set to be 0. Our model clearly demonstrates that the circadian period of WT MEFs and INK4a/ARF$^{-/-}$ MEFs are almost the same (23.65 hours vs 23.69 hours) when RAS is normally expressed ($ktt=1$), however, as ktt decreases, a longer circadian period is observed in WT system while the INK4a/ARF$^{-/-}$ system shows a shorter period in comparison with their corresponding control (Figure 17A). This result is in consistence with the experimental observations shown in Section 3.1. It is interesting to note that INK4a/ARF$^{-/-}$ system reaches its shortest period when $ktt=0.6$ and the period becomes longer in response to higher-levels of RAS ($0<ktt<0.6$). Similar phenomena was observed in experiments (data not shown), but the underlying mechanism has not been elucidated at this stage. For a better interpretation of the experimental data, we used $ktt=0.6$ to model RAS overexpression in the present work.

In order to compare the expression features (i.e. magnitude and phase) of *Bmal*, which is a central node in the circadian network and is commonly used as a reference when we study the period of the system, we plotted its absolute mRNA expression patterns in WT and INK4a/ARF$^{-/-}$ MEFs without being normalized to the average values. From Figure 17B, it can be observed that the expression level is slightly higher and an obvious phase shift can be measured when we compare *in silico Bmal* expression patterns in INK4a/ARF$^{-/-}$ MEFs with that in WT MEFs. We speculate that the difference between the phases of *Bmal* in WT and INK4a/ARF$^{-/-}$ MEFs might have an influence on the different changes in circadian period upon RAS perturbation. The values of the periods and phases of WT and INK4a/ARF$^{-/-}$ MEFs under normal conditions as well as the periods of these two systems upon RAS overexpression are given in Table 2. The comparison of model simulations with experimental data suggests that our model can be used to preliminarily interpret the experimental results.

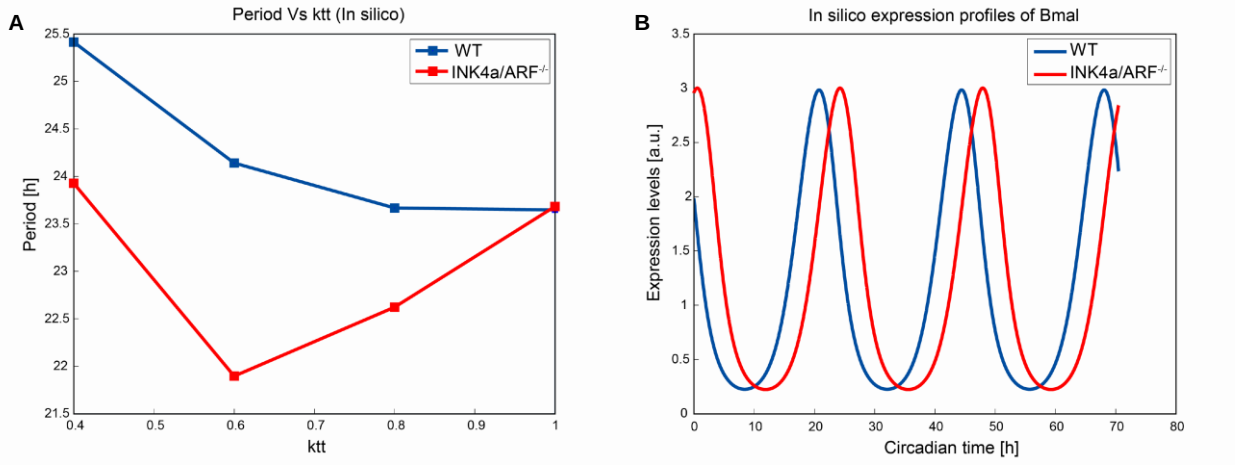

Figure 17: In *silico* data of circadian periods and *Bmal* expression profiles of WT and INK4a/ARF$^{-/-}$ systems (unpublished data, manuscript in preparation). (A) Shown are values of the periods of WT (blue) and INK4a/ARF$^{-/-}$ (red) systems upon RAS overexpression ($ktt<1$). **(B)** The comparison of *in silico* expression profiles of *Bmal* in WT (blue) system and INK4a/ARF$^{-/-}$ (red)

systems over around 3 days without RAS perturbations.

Table 2: Corresponding values of the phases and periods of original and extended models shown in Figure 16B.

	Control (ktt=1)		+RAS (ktt=0.6)
	Phase (CT) [hours]	Period [hours]	
wild-type	21	23.65	24.14
INK4a/ARF$^{-/-}$	23.95	23.69	21.9

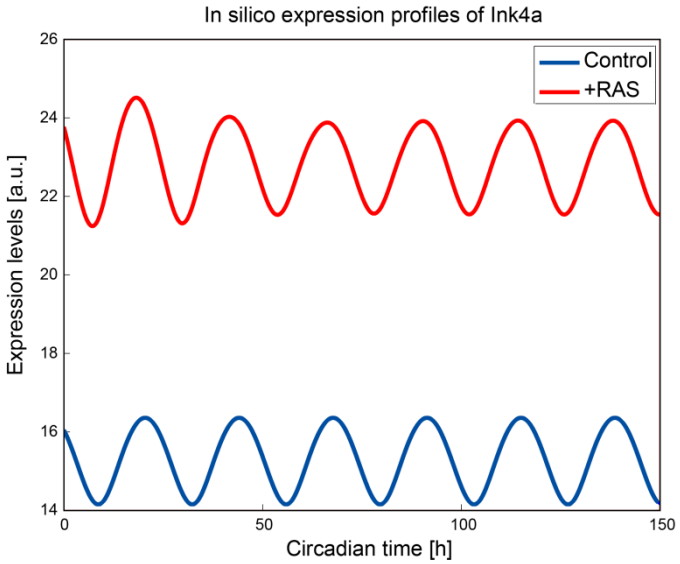

Figure 18: In *silico* expression profiles of *Ink4a* over 6 days obtained using the extended model (unpublished data, manuscript in preparation). The blue curve represents the expression under non-perturbed condition and the red curve represents the expression upon RAS overexpression.

3.3.3 Comparison between computational predictions and microarray data

Microarray technology provides an efficient way to monitor gene expression levels at a large scale under different conditions. To further explore the effect of RAS overexpression on the core circadian clock, the gene expression data of WT and INK4a/ARF$^{-/-}$ MEFs with and without H-RAS overexpression were analyzed in our group. At this stage, the absolute log2 fold change cutoff was preliminarily set to 1. Interestingly, all the five core-clock genes are not considered to be significantly differentially expressed in WT MEFs upon H-RAS overexpression (the absolute value of fold change is less than 1), while in INK4a/ARF$^{-/-}$ MEFs the log2 fold changes of *Per3* and *Rorα* are -1.02 and 1.43, respectively, in response to H-RAS overexpression.

Computational predictions of expression profiles of core-clock genes upon RAS overexpression in WT and INK4a/ARF$^{-/-}$ situations were carried out with our extended model and assessed against the microarray data. The average value of the *in silico* expression level of each gene over 3 days were taken and compared with the microarray data (single-time-point). From Figure 20, we noticed that the expression levels of *Per* and *Ror* were increased when RAS is overexpressed (ktt=0.6) in INK4a/ARF$^{-/-}$ system, which is consistent with the microarray data. It is interesting to notice that while RAS

overexpression does not have much influence on the phases of core-clock genes in WT system, clear shifts are observed in the *in silico* expression peaks of all the five core-clock genes upon RAS overexpression in INK4a/ARF$^{-/-}$ system.

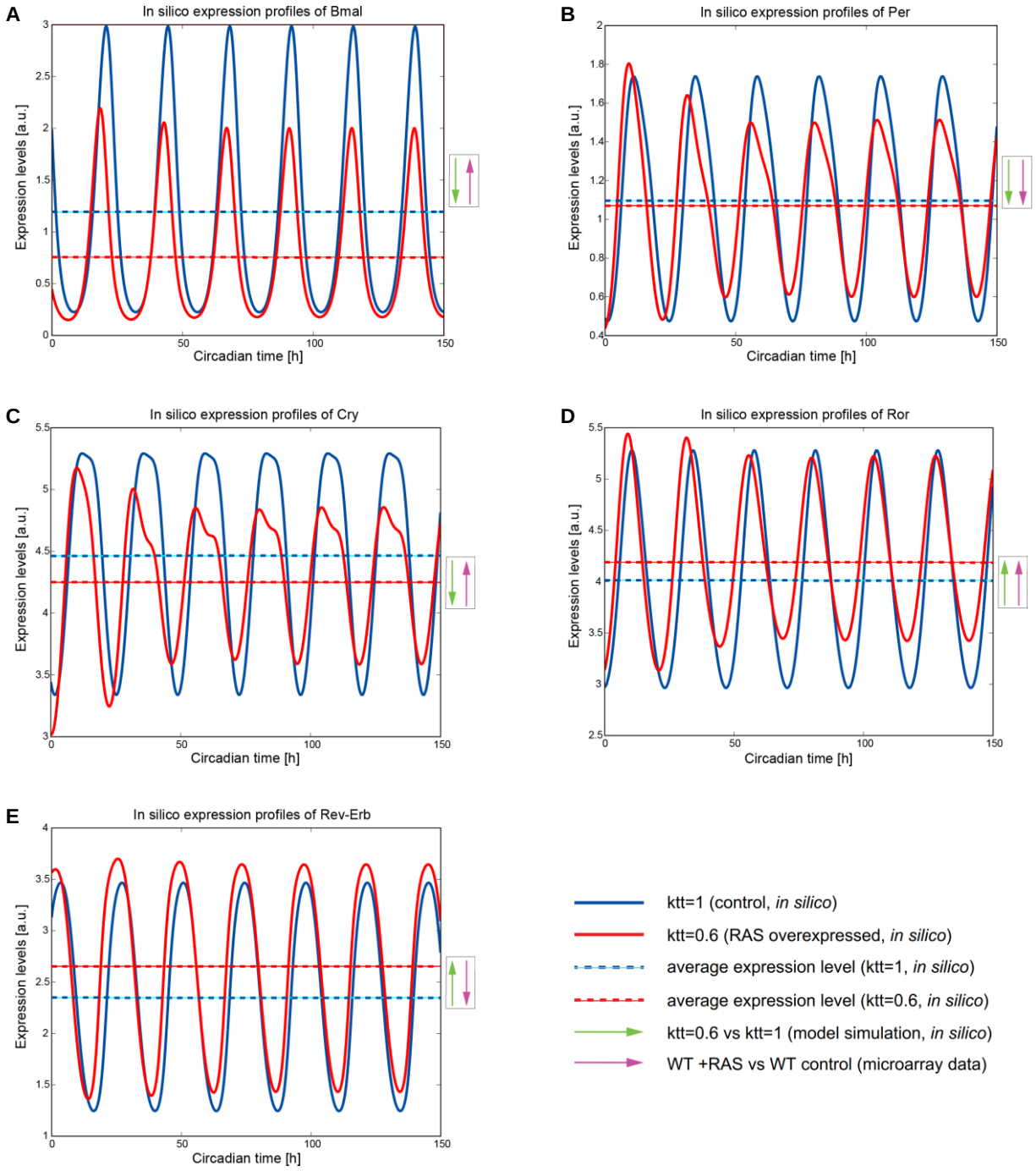

Figure 19: In *silico* expression profiles of core-clock genes in WT system upon RAS overexpression simulated with the extended model over 6 days (unpublished data, manuscript in preparation). The blue and red solid lines represent the expressions in the control situation (without perturbation of RAS, $ktt=1$) and upon RAS overexpression ($ktt=0.6$), respectively. The blue and red dashed lines indicate the corresponding average values of the expression levels. The green arrows, which always point from the blue dashed lines to the red dashed lines, represent the

directions of the changes in the average expression levels upon RAS overexpression compared to their corresponding control based on *in silico* data. Although none of the core-clock genes are considered to be differentially expressed upon the induction of H-RAS according to microarray data, the trend of their changes are represented by purple arrows shown in the figure.

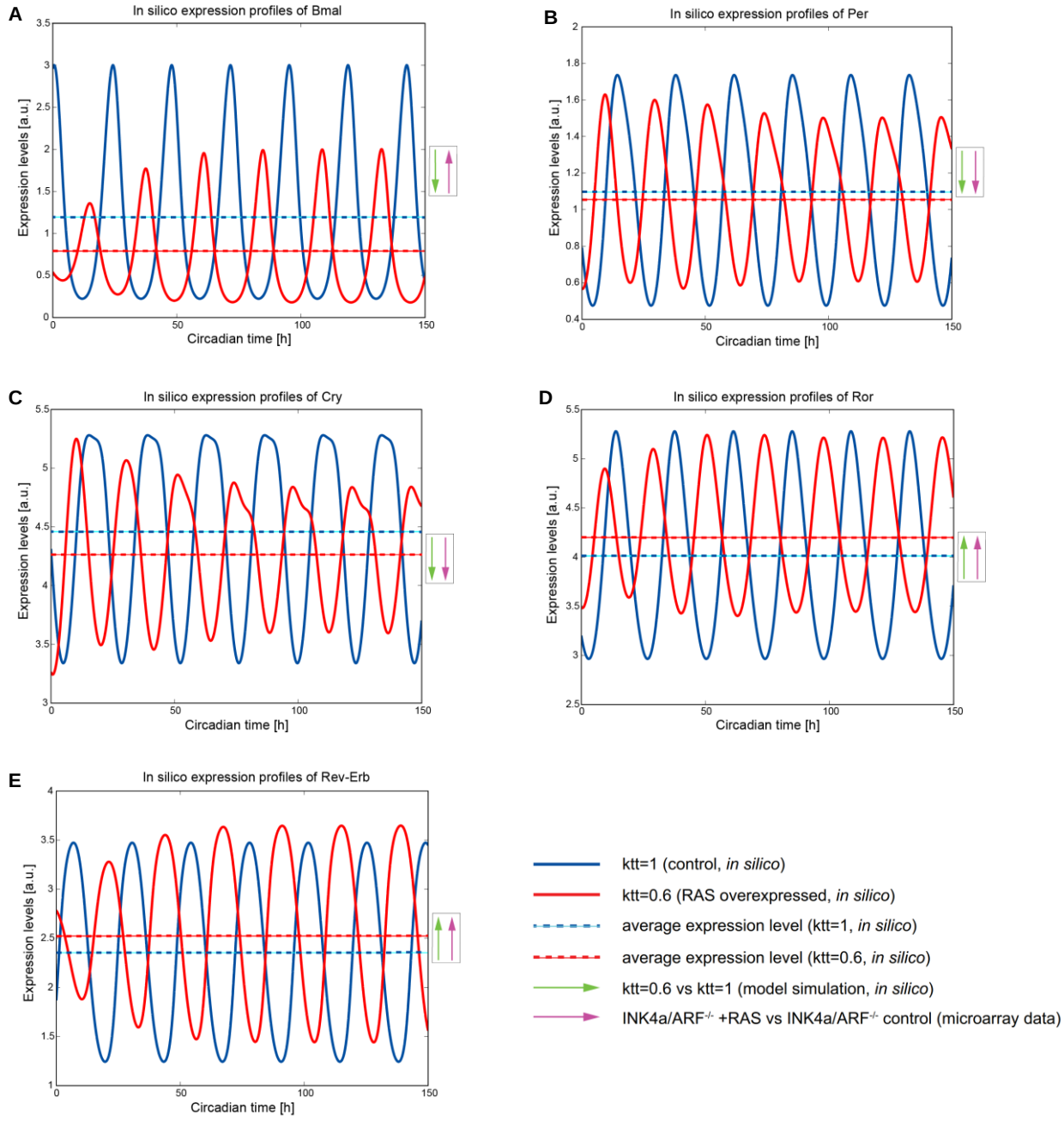

Figure 20: In *silico* expression profiles of core-clock genes in INK4a/ARF$^{-/-}$ system upon RAS overexpression simulated with the extended model over 6 days (unpublished data, manuscript in preparation). The annotation is the same as the one in Figure 18. Based on the microarray datasets of INK4a/ARF$^{-/-}$ MEFs, the absolute log2 fold changes of *Per3* (*Per* in the model) and *Rorα* (*Ror* in the model) are larger than 1 upon the induction of H-RAS.

To further test the model, we also simulated the expressions of core-clock genes with *Bmal* knocked-down, which was achieved by reducing the value of parameter i (the activation of *Bmal*) to 50% (Eq. (34)). From the *in silico* expression profiles (Figure 21), we observed an increase in the average expression levels of *Per* and *Cry* and a decrease in the expression of *Ror* and *Rev-Erb*. These predictions was compared to the microarray data obtained from WT MEFs with and without shBmal introduced, where the two Rev-Erb nuclear orphan receptors (*Rev-Erbα, Rev-Erbβ*) were shown to be downregulated with log2 fold changes of -1.85 and -2.38, respectively, upon the introduction of shBmal. It is worth noting that the changes in the *in silico* expression of all the five core-clock genes follow the same direction as that observed in microarray data. These results suggest that our predictions could be qualitatively verified by the microarray data. However, a more careful statistical analysis is required to determine a suitable fold change cutoff and p-value cutoff for identifying significantly differentially expressed genes.

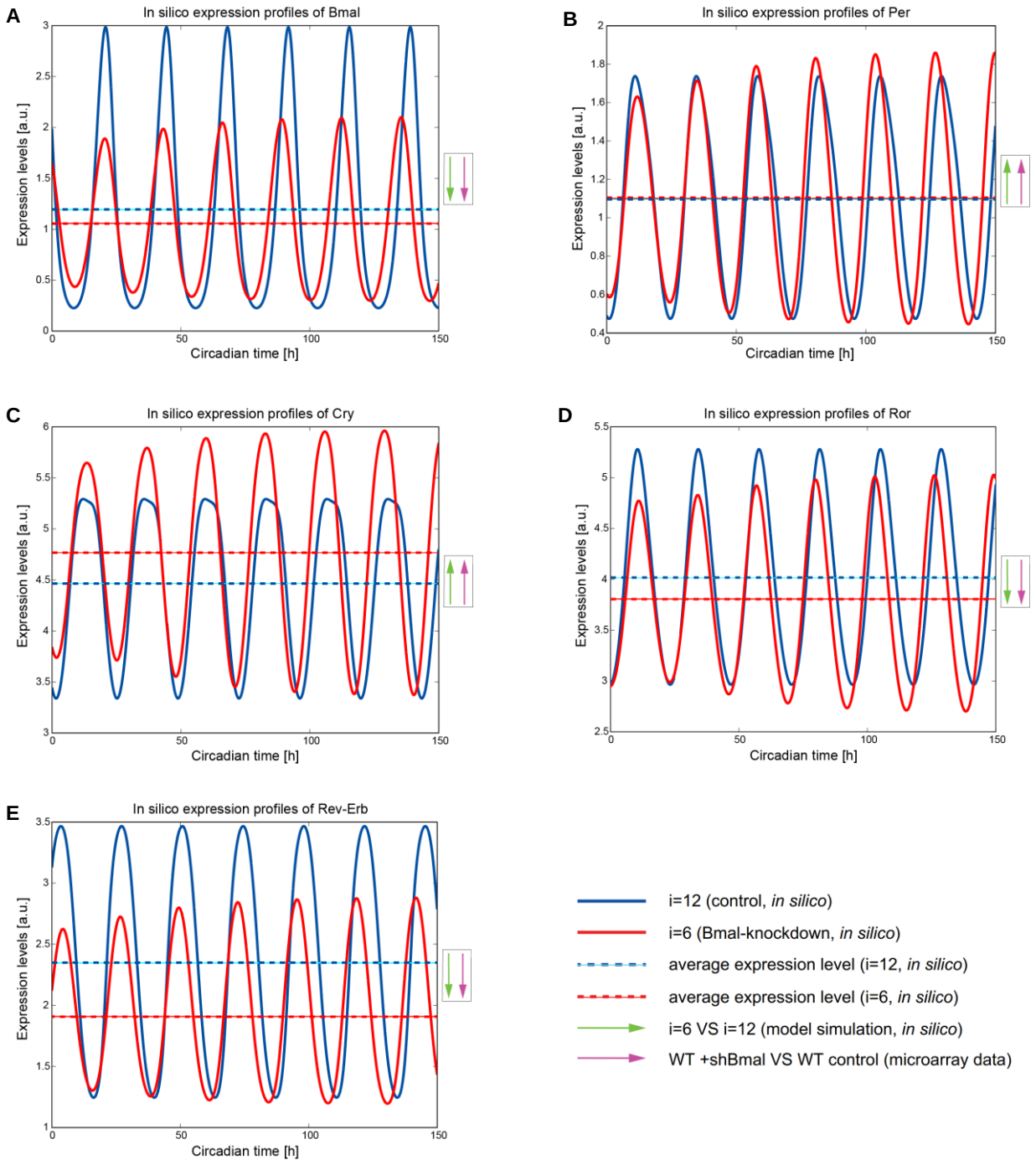

Figure 21: In *silico* expression profiles of core-clock genes in WT system upon the knockdown of *Bmal* simulated with the extended model over 6 days (unpublished data, manuscript in preparation). The annotation of this figure is similar to the one of Figure 18 but adjusted to the perturbation of *Bmal* knockdown. The absolute log2 fold changes of *Rev-Erbα, Rev-Erbβ* (represented by *Rev-Erb* in the model) are larger than 1 upon the introduction of shBmal according to microarray datasets.

3.3.4 Modular analysis

In order to investigate the relative influence of INK4a-CDK-Rb-E2F and ARF-MDM2-p53 in mediating RAS-induced effect on circadian clock, we decided to test if the presence and oscillation of both of them are necessary to reproduce the experimental data on the circadian period of WT and INK4a/ARF$^{-/-}$ MEFs (shown in Section 3.1). In this Section, the INK4a-CDK-Rb-E2F pathway is referred to as Module 1 and ARF-MDM2-p53 pathway is referred to as Module 2 (Figure 22).

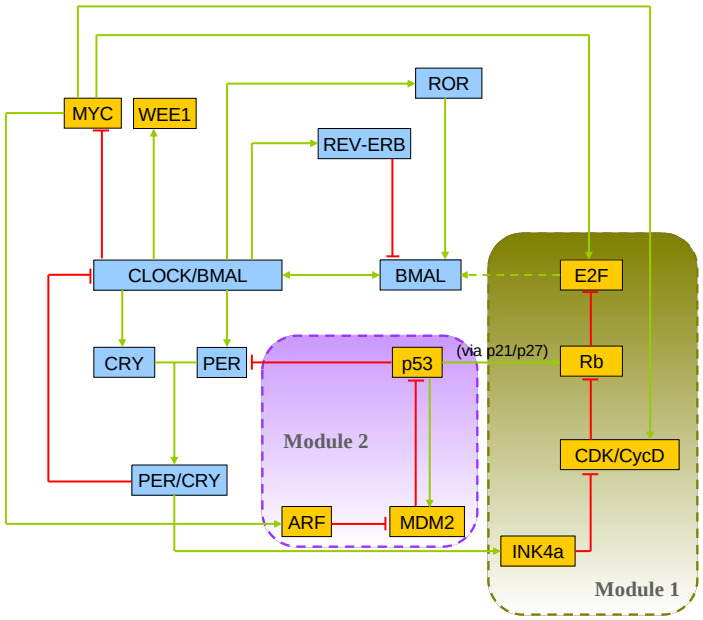

Figure 22: Simplified schematic diagram of the extended network with the INK4a-CDK-Rb-E2F module and the ARF-MDM2-p53 module highlighted. The INK4a-CDK-Rb-E2F pathway (Module 1) is highlighted in green and the ARF-MDM2-p53 pathway (Module 2) is highlighted in purple.

From the schema of the network, we can see that the inductive effect of E2F on the transcription of *Bmal* is the only connection from Module 1 to the core circadian clock. In *silico*, it is sufficient to remove the feedback effect from Module 1 on the core circadian clock by setting the concentration of E2F nuclear protein ($E2F_N$) to 0, which is achieved by setting its initial condition and the rate of change of its concentration (Eq. (29)) to 0. The expression levels of the nuclear proteins of the components in Module 1 after setting $E2F_N=0$ are shown in Figure 23-A. Here, we modeled the INK4a/ARF$^{-/-}$ system by setting the concentration of *Arf* (Eq. (21)), ARF_c (Eq. (22)), ARF_N (Eq. (23)) to 0, as the influence of INK4a has already been removed from the system. It can be observed in Figure 23B that both WT and INK4a/ARF$^{-/-}$ systems show shorter periods upon RAS overexpression ($ktt=0.6$) compared to normal conditions ($ktt=1$), which is different from experimental observations and our simulations with the presence of Module 1. We further investigated the role of the oscillation of Module 1 in RAS-induced effect on circadian period. The oscillatory expression of $E2F_N$ was replaced with its average value (Figure 23C), which is achieved by setting the initial condition of $E2F_N$ concentration to the mean value of its oscillatory (5.7 [a.u.]) and the rate of change (Eq. (29)) to 0. In this case, similar deregulated circadian phenotypes are observed in WT and INK4a/ARF$^{-/-}$ systems:

both of them exhibit a shorter period when RAS is slightly overexpressed ($0.8 \leq ktt \leq 1$) while their periods become longer upon the introduction of larger amount of RAS ($0 < ktt < 0.8$), which is also not consistent with the experimental data. These results confirm that both the presence and oscillation of Module 1 are crucial for RAS-induced effect on the circadian period.

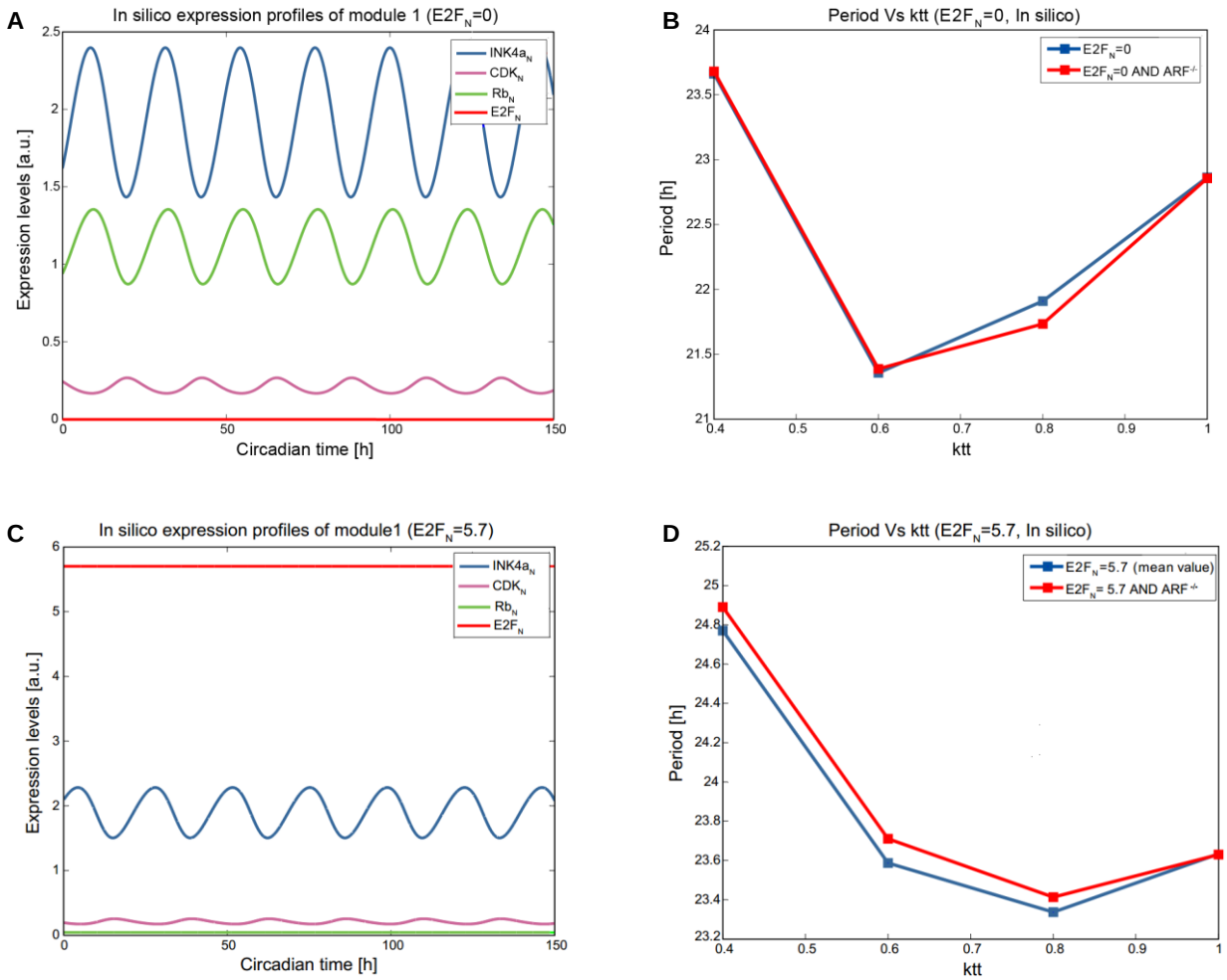

Figure 23: The relevance of Module 1 to period phenotypes (unpublished data, manuscript in preparation). (**A**) and (**C**) are *in silico* expression profiles of nuclear proteins of the genes (INK4a$_N$: blue, CDK$_N$: purple, Rb$_N$: green, E2F$_N$: red) in Module 1 when the concentration of E2F$_N$ is set to 0 and to its average expression level, respectively. (**B**) and (**D**) are the corresponding period phenotypes to (**A**) and (**C**). The blue lines represent the periods of *Bmal* when the concentration of E2F$_N$ is set to 0 (**B**) and to its average expression level (**D**), while the red lines represent the periods when ARF is knocked-out in these situations.

Similarly, we carried out a set of simulations regarding the role of Module 2 in RAS-induced effect on circadian period. Module 2 is connected to the core circadian clock via p53-*Per* interaction and the p53-Rb-E2F arm. In order to test if the presence of Module 2 is essential for mediating RAS-induced effect on circadian period, the concentration of p53$_N$ (both the initial condition and Eq. (38)) was set to 0. In this case, the INK4a/ARF$^{-/-}$ system was modeled by setting the concentration of *Ink4a,* INK4a$_c$,

INK4a$_N$ to 0. As shown in Figure 24 B, WT system shows a shorter period upon RAS overexpression (ktt=0.6), which is not consistent with the experimental observations shown in Section 3.1, indicating that Module 2 is important in RAS-induced circadian dysfunction and the absence of Module 2 leads to a change in circadian response of WT MEFs upon RAS overexpression. Interestingly, when the oscillatory expression of Module 2 was replaced by a constant expression (the expression level of p53$_N$ was set to 0.56 [a.u.], which is the average value of its original oscillations), both of the WT system and INK4a/ARF$^{-/-}$ system showed similar circadian phenotypes to the corresponding experimental observations: WT system exhibits a longer circadian period while the a shorter period is shown in INK4a/ARF$^{-/-}$ system upon RAS overexpression (Figure 24 D), suggesting that the oscillation of Module 2 plays a minor role in influencing the changes of MEF's period in response to RAS overexpression.

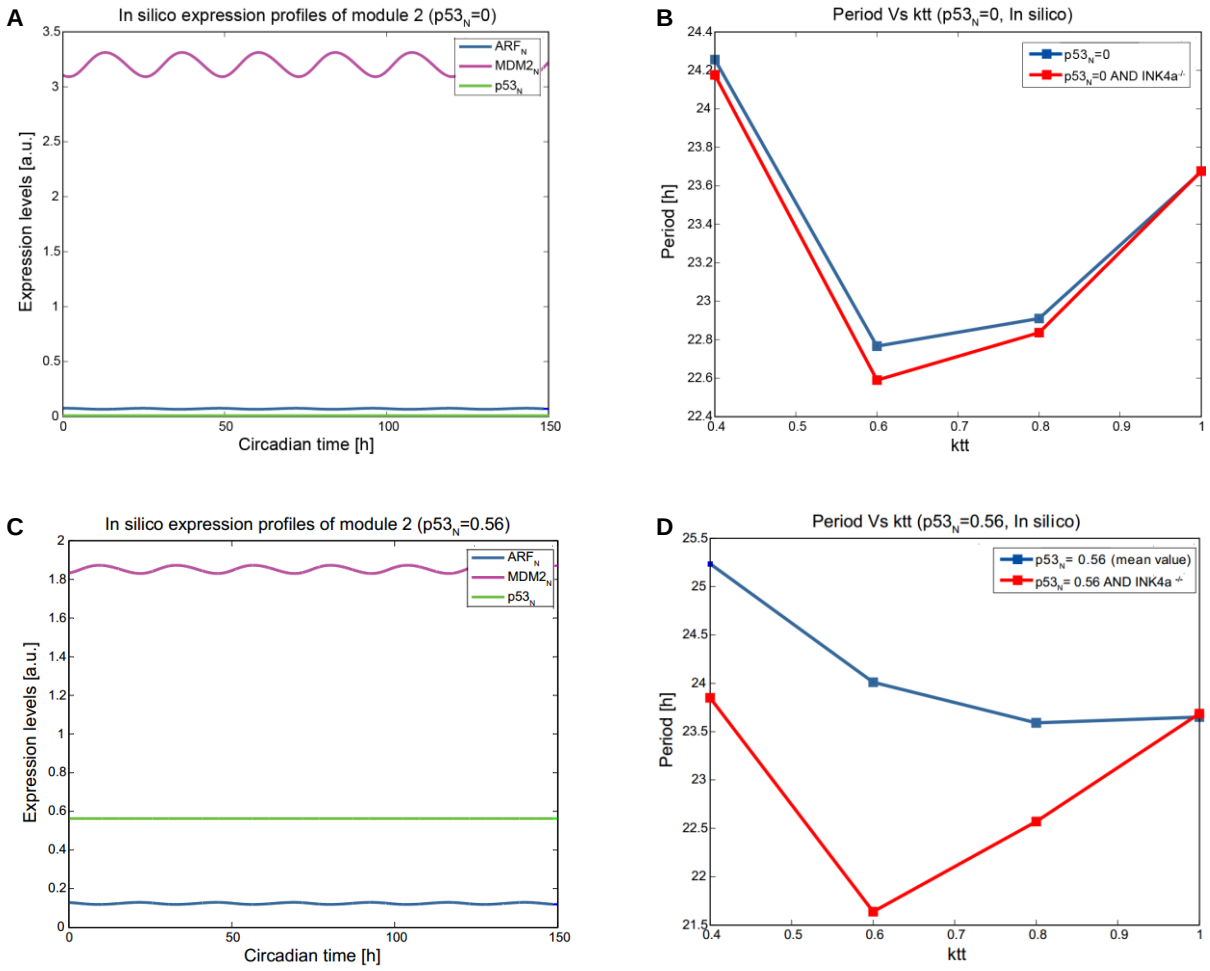

Figure 24: The relevance of Module 2 to period phenotypes (unpublished data, manuscript in preparation). (**A**) and (**C**) are *in silico* expression profiles of nuclear proteins of the genes (ARF$_N$: blue, MDM2$_N$: purple, p53$_N$: green) in Module 2 when the concentration of E2F$_N$ is set to 0 and its average expression level, respectively. (**B**) and (**D**) are the corresponding period phenotypes to (**A**) and (**C**). The blue lines represent the periods of *Bmal* when the concentration of p53$_N$ is set to 0 (**B**) and to its average expression level (**D**), while the red lines represent the periods when INK4a is knocked-out in these situations.

3.3.5 Model predictions

3.3.5.1 Model predictions of circadian phenotypes of $ARF^{-/-}$, $INK4a^{-/-}$, $Rb^{-/-}$, $E2F^{-/-}$ MEFs

The goal of mathematical models is not only to interpret the available experimental data but also to provide predictions and guide experiments that will in turn validate the model predictions. In order to study the role of ARF, INK4a, Rb and E2F in regulating circadian clock individually, a set of predictions have been made with the newly extended model in this section, showing the circadian characteristics of $ARF^{-/-}$, $INK4a^{-/-}$, $Rb^{-/-}$, $E2F^{-/-}$ MEFs. Each of these knockout systems was modeled by setting the initial conditions of the mRNA, cyctoplasmic protein and nuclear protein of the gene, and the rate of change of their concentration to 0. The *in silico* expression profiles of *Bmal* mRNA and nuclear protein ($BMAL_N$) are shown in Figure 25 and these predictions can be further experimentally tested in $ARF^{-/-}$, $INK4a^{-/-}$, $Rb^{-/-}$ MEFs, which are available in our group.

It can be noticed that the knockout of ARF does not make much difference in circadian phenotypes, including period and peak phase (Figure 24 A-B). The *in silico* circadian phenotypes of $INK4a^{-/-}$ system and $Rb^{-/-}$ system are similar, showing delayed phases of *Bmal* mRNA and nuclear protein compared to the WT system while the periods and expression level are almost unchanged (Figure 24 C-F). These simulations confirm the experimental data which shows the INK4a/$ARF^{-/-}$ MEFs has similar period with WT MEFs (Section 3.1), indicating that ARF and INK4a themselves do not have much effect on the circadian clock independent of RAS perturbation. However, the $E2F^{-/-}$ system showed a more obvious dysfunctional circadian phenotype: a lower expression level of both *Bmal* mRNA and nuclear protein, a shorter period (22.86 hours vs 23.65 hours) and a delayed phase of approximately 4.5 hours later than in WT systems.

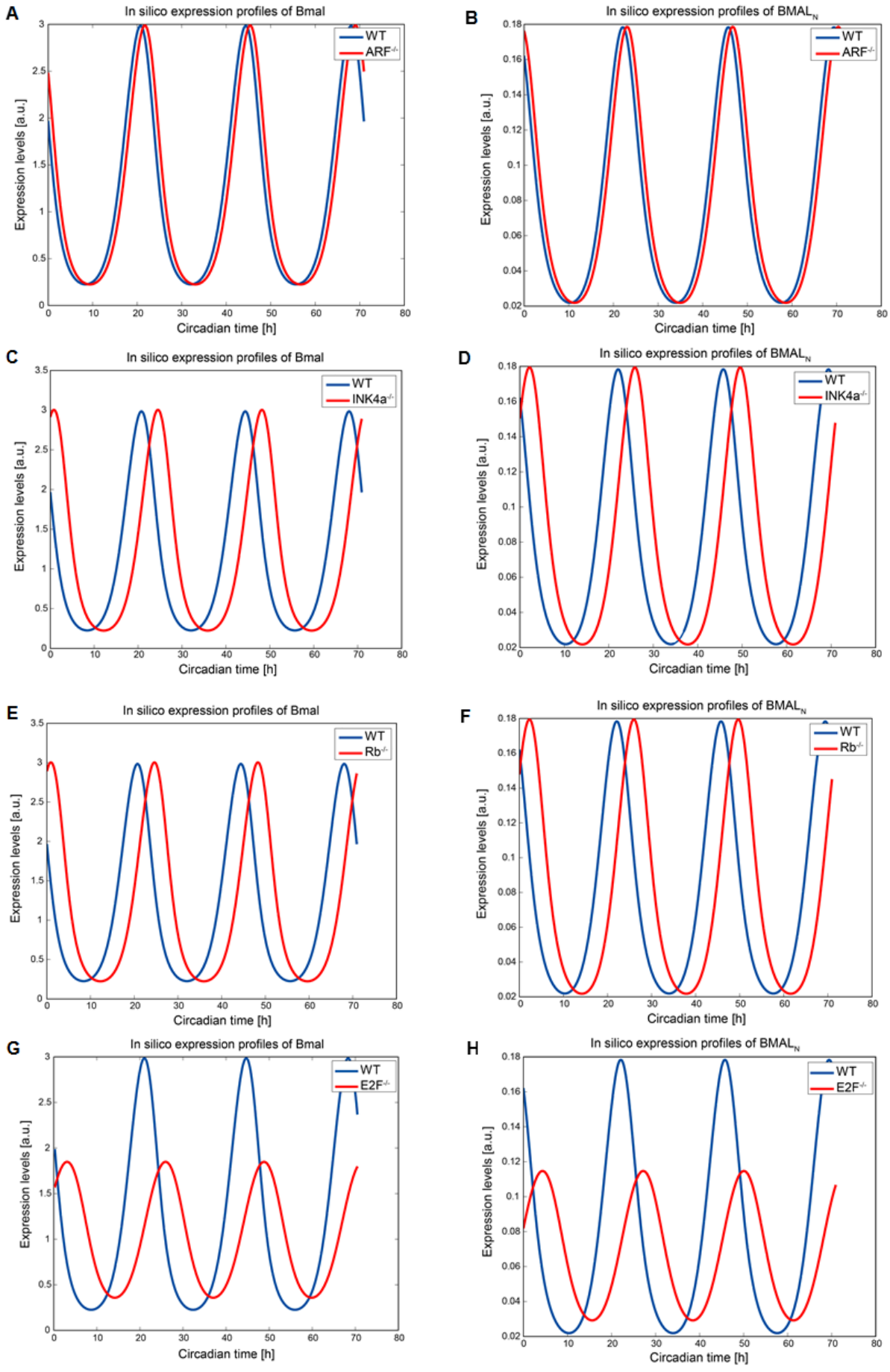
A
In silico expression profiles of Bmal
WT
ARF-/-
Expression levels [a.u.]
Circadian time [h]
B
In silico expression profiles of BMAL$_N$
WT
ARF-/-
Expression levels [a.u.]
Circadian time [h]
C
In silico expression profiles of Bmal
WT
INK4a-/-
Expression levels [a.u.]
Circadian time [h]
D
In silico expression profiles of BMAL$_N$
WT
INK4a-/-
Expression levels [a.u.]
Circadian time [h]
E
In silico expression profiles of Bmal
WT
Rb-/-
Expression levels [a.u.]
Circadian time [h]
F
In silico expression profiles of BMAL$_N$
WT
Rb-/-
Expression levels [a.u.]
Circadian time [h]
G
In silico expression profiles of Bmal
WT
E2F-/-
Expression levels [a.u.]
Circadian time [h]
H
In silico expression profiles of BMAL$_N$
WT
E2F-/-
Expression levels [a.u.]
Circadian time [h]

Figure 25: In *silico* expression profiles of *Bmal* and $BMAL_N$ obtained from simulations with the extended model over 3 days (unpublished data, manuscript in preparation). The blue curves represent the expressions in WT system and the red curves represent expressions in different perturbed systems: $ARF^{-/-}$ system (**A-B**), $INK4a^{-/-}$ system (**C-D**), $Rb^{-/-}$ system (**E-F**), $E2F^{-/-}$ system (**G-H**).

3.3.5.2 Model prediction of the effect of adriamycin on the period

Adriamycin is an anticancer drug, which promotes cellular senescence to inhibit the proliferation of tumor cells, commonly used in the treatment of several types of cancer (e.g. lung cancer, breast cancer, etc.) [73]. It has been reported that p53 is upregulated in the breast tumor cells exposed to adriamycin and it plays an important role in mediating adriamycin-induced senescence [74]. In order to investigate if the upregulation of p53 resulting from adriamycin treatment disrupts the circadian clock, we carried out a simulation where we overexpress p53 nuclear protein by 12 fold (Eq. (38), $souce\_p53_{new}=54$), and identify the corresponding effect on the period of the system. From the *in silico* expression profile of *Bmal* shown in Figure 26A, we can see that the overexpression of p53 leads to an increase in the period of the system (24.05 hours VS 23.65 hours). This prediction is in agreement with the preliminary experimental data in our group: the 0.01 mg/ml adriamycin treated MEFs showed a longer period compared to the corresponding control (Figure 26 B-C).

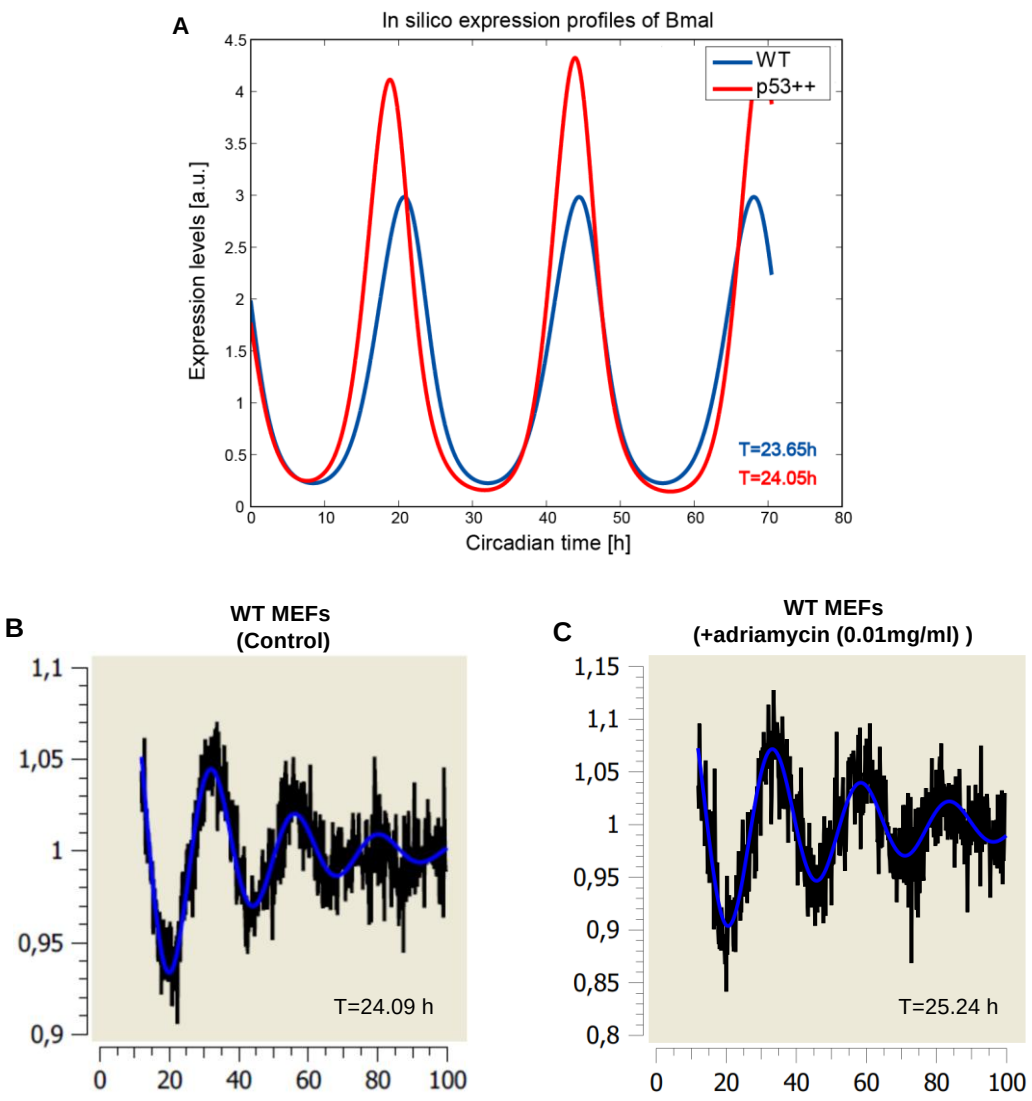

Figure 26: In *silico* and experimental analysis of the effect of adriamycin induction on circadian period (unpublished data, manuscript in preparation). (**A**) In *silico* expression profiles of *Bmal* obtained from simulations with the extended model. The blue curve represents non-perturbed situation (T=23.65 hours) and the red curve represents the result when p53 is 12-fold overexpressed. (**B-C**) Experimental analysis of circadian period of WT MEFs treated with 0.01mg/ml adriacycin (unpublished data, manuscript in preparation) (**B**) in comparison with that in non-perturbed situation (**A**). The black line is the trendeliminated data and the blue line is the fit by ChronoStar analysis software.

4. Discussion

Accumulating experimental evidence shows that the mammalian circadian clock is associated with various of cellular processes involved in cancer control, such as cell cycle regulation [2], DNA damage responses [3] and metabolism [4]. However, the exact mechanisms linking the circadian system and these processes are poorly understood. Mathematical models can be of great help to gain a qualitative understanding of the underlying pathways and interactions. In this project, we extended the group's previously developed mathematical model for the mammalian core-clock to output genes and pathways which are considered to be crucial in the regulation of Ras-induced proliferation control.

Our newly extended model maintained the robust circadian oscillations of the system and it achieved the optimal relative phase relations between the core-clock components. The model was used to interpret the experimental data produced in a MEFs cell system in our group, where WT MEFs and INK4a/ARF$^{-/-}$ MEFs showed opposite circadian phenotypes upon RAS overexpression. In agreement with the experimental observations, the extended model shows that WT MEFs exhibited an increased period, whereas their INK4a/ARF$^{-/-}$ counterparts obtained an shorter period upon RAS overexpression, suggesting that INK4a and ARF play crucial roles in RAS-mediated effect on the circadian system. It is interesting to notice that the effect of RAS overexpression on the period of INK4a/ARF$^{-/-}$ MEFs is non-monotonic: first a decrease is observed in the period when a small amount of RAS is overexpressed, and subsequently the period is increased in response to a higher-level of RAS. This behavior is similar to the effect of *Per* perturbation on the period: both downregulation and overexpression of *Per* can lead to a shorter circadian period, which was shown theoretically and experimentally in the previous studies [9, 75, 76]. More efforts are need to elucidate the underlying mechanisms of this non-monotonic behavior.

In this extended model, we included two feedbacks from the external genes, INK4a and ARF, to the core circadian clock. One of these feedbacks is the INK4a-CDK/CycD-Rb-E2F-Bmal pathway. A potential binding site for E2F activators within the promoter region of *Bmal1* has been reported by the MotifMap database based on motif analysis [40], which suggests that E2F activators could induce the transcription of *Bmal1*. However, we have not found explicit experimental evidences for this potential transactivation. Our *in silico* data shows that the E2F$^{-/-}$ MEFs obtain a dysfunctional circadian phenotypes with a shorter period, a delayed phase and a lower expression level of *Bmal*. Experiments will be carried out to validate the correlation between E2Fs and the expression of *Bmal1*, the effect of E2Fs on the circadian system will also be studied experimentally in our group.

Apart from the determination of reaction mechanisms and model structure, the parameter estimation is another challenge in modeling of biological systems, as the value of parameters can also affect the network behaviors. For the newly included interactions in the present model, some parameters, such as the degradation rates of nuclear protein components, Michaelis-Menten constants were retrieved from the literature. The phosphorylation/dephosphorylation rates, protein complex formation/dissociation rates were set to the reported typical values for similar kinetic processes. However, there are still many parameters remaining free: the hill coefficients were set to 1 at this stage; for other free parameters, the average value of the same type of parameters in the pre-

existing core-clock model was used, additionally some of them were fine-tuned to fit our experimental observations. Consequently, our model was qualitatively verified by experimental data, but it is not at this stage a precise quantitative model. Further efforts are needed to determine the parameters precisely in a systematic way, such as using control theory based on published experimental data of amplitudes and phases.

The *in silico* expression profiles of core-clock genes obtained from simulations with the extended model were compared with and qualitatively verified by available microarray data in our group. In our microarray data analysis, the cutoff of absolute log2 fold change was preliminarily set to 1. The difference of the expression levels of core-clock genes was studied under different conditions: upon RAS overpression in WT MEFs and INK4a/ARF$^{-/-}$ MEFs, upon the introduction of shBmal in WT MEFs. Remarkably, the changes of expression of all core-clock genes with a absolute value of log2 fold change larger than 1 observed in microarray data follow the same direction as that shown in our computational predictions. However, it is need to be noted that the statistical tests are still required to determine a suitable fold change cutoff and p-value cutoff for identifying significantly differentially expressed genes.

Published data shows that the intake of anticancer drugs can influence the circadian system and the circadian disruption leads to a poorer prognosis [77]. It is known that the anticancer drug adriamycin can induce the expression of the tumor suppressor p53. Here, we studied the effect of the accelerated expression of p53 on the circadian period using the simulations with our extend model. As it is mentioned in Section 3.3.4, our *in silico* data shows that when the concentration of p53 protein is increased by 12 fold, the system exhibits a longer period, which is consistent with the observations in our preliminary experiments where the MEFs was treated with 0.01 mg/ml adriamycin. Furthermore, we carried out a series of simulations where we overexpress p53 protein by different folds (Eq. (38)), and we noticed that the system exhibits disrupted period upon different perturbations of p53 but the effect is non-monotonic: with a continuous increase of p53, it is first observed a shorter period and subsequently a longer period (Figure 27), indicating that the effect of adriamycin on the circadian period is concentration-dependent. Further experiments will be carried out to test this prediction and it might be helpful for optimizing the treatment with adriamycin.

Together, our extended model was qualitatively verified by available experimental data in our group and it can generate testable predictions, which inspire new experiments. This work may represent a step towards understanding the interplay between mammalian circadian clock and control of proliferation.

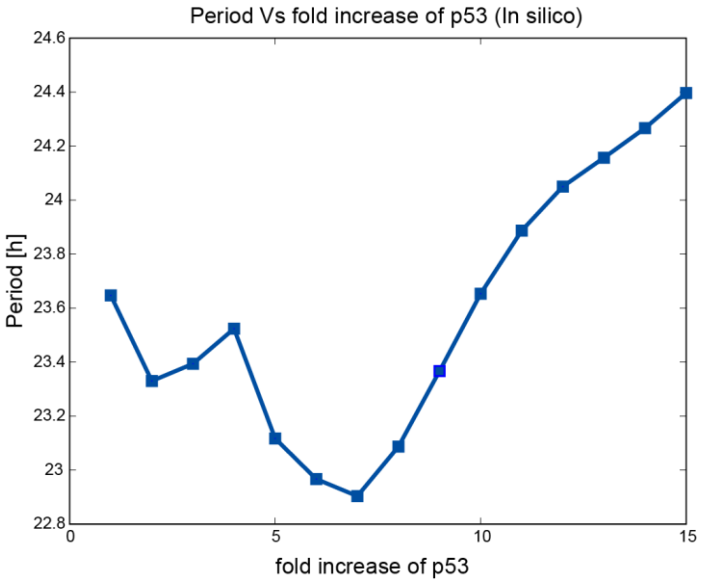

Figure 27: Effect of p53 overexpression on circadian period of MEFs (*in silico*). Shown are predicted changes in the period of MEFs upon p53 overexpression.

References

[1] Roenneberg T, Merrow M. Circadian clocks - the fall and rise of physiology. Nat Rev Mol Cell Biol 2005;6:965-71.

[2] Borgs L, Beukelaers P, Vandenbosch R, Belachew S, Nguyen L, Malgrange B. Cell "circadian" cycle: new role for mammalian core clock genes. Cell Cycle 2009;8:832-7.

[3] Gaddameedhi S, Reardon JT, Ye R, Ozturk N, Sancar A. Effect of circadian clock mutations on DNA damage response in mammalian cells. Cell Cycle 2012;11:3481-91.

[4] Nakahata Y, Sahar S, Astarita G, Kaluzova M, Sassone-Corsi P. Circadian control of the NAD+ salvage pathway by CLOCK-SIRT1. Science 2009;324:654-7.

[5] Reppert SM, Weaver DR. Coordination of circadian timing in mammals. Nature 2002;418:935-41.

[6] Buijs RM, Scheer FA, Kreier F, Yi C, Bos N, Goncharuk VD, et al. Organization of circadian functions: interaction with the body. Prog Brain Res 2006;153:341-60.

[7] Bollinger T, Schibler U. Circadian rhythms - from genes to physiology and disease. Swiss Med Wkly 2014;144:w13984.

[8] Ueda HR, Hayashi S, Chen W, Sano M, Machida M, Shigeyoshi Y, et al. System-level identification of transcriptional circuits underlying mammalian circadian clocks. Nat Genet 2005;37:187-92.

[9] Relogio A, Westermark PO, Wallach T, Schellenberg K, Kramer A, Herzel H. Tuning the mammalian circadian clock: robust synergy of two loops. PLoS Comput Biol 2011;7:e1002309.

[10] Zhang EE, Kay SA. Clocks not winding down: unravelling circadian networks. Nat Rev Mol Cell Biol 2010;11:764-76.

[11] Huang N, Chelliah Y, Shan Y, Taylor CA, Yoo SH, Partch C, et al. Crystal structure of the heterodimeric CLOCK:BMAL1 transcriptional activator complex. Science 2012;337:189-94.

[12] Guillaumond F, Dardente H, Giguere V, Cermakian N. Differential control of Bmal1 circadian transcription by REV-ERB and ROR nuclear receptors. J Biol Rhythms 2005;20:391-403.

[13] Fan Y, Hida A, Anderson DA, Izumo M, Johnson CH. Cycling of CRYPTOCHROME proteins is not necessary for circadian-clock function in mammalian fibroblasts. Curr Biol 2007;17:1091-100.

[14] Yamamoto Y, Yagita K, Okamura H. Role of cyclic mPer2 expression in the mammalian cellular clock. Mol Cell Biol 2005;25:1912-21.

[15] Tyson JJ, Novak B. Temporal organization of the cell cycle. Curr Biol 2008;18:R759-R68.

[16] Morgan DO. Principles of CDK regulation. Nature 1995;374:131-4.

[17] Mitchison TJ, Salmon ED. Mitosis: a history of division. Nat Cell Biol 2001;3:E17-21.

[18] Elledge SJ. Cell cycle checkpoints: preventing an identity crisis. Science 1996;274:1664-72.

[19] Unsal-Kacmaz K, Mullen TE, Kaufmann WK, Sancar A. Coupling of human circadian and cell cycles by the timeless protein. Mol Cell Biol 2005;25:3109-16.

[20] Hayflick L. THE LIMITED IN VITRO LIFETIME OF HUMAN DIPLOID CELL STRAINS. Exp Cell Res 1965;37:614-36.

[21] Braig M, Schmitt CA. Oncogene-induced senescence: putting the brakes on tumor development. Cancer Res 2006;66:2881-4.

[22] Munoz-Espin D, Serrano M. Cellular senescence: from physiology to pathology. Nat Rev Mol Cell Biol 2014;15:482-96.

[23] Campisi J, d'Adda di Fagagna F. Cellular senescence: when bad things happen to good cells. Nat Rev Mol Cell Biol 2007;8:729-40.

[24] Ben-Porath I, Weinberg RA. The signals and pathways activating cellular senescence. Int J Biochem Cell Biol 2005;37:961-76.

[25] Collado M, Serrano M. Senescence in tumours: evidence from mice and humans. Nat Rev Cancer 2010;10:51-7.

[26] Courtois-Cox S, Jones SL, Cichowski K. Many roads lead to oncogene-induced senescence. Oncogene 2008;27:2801-9.

[27] Schmitt CA. Senescence, apoptosis and therapy--cutting the lifelines of cancer. Nat Rev Cancer 2003;3:286-95.

[28] Perez-Roger I, Kim SH, Griffiths B, Sewing A, Land H. Cyclins D1 and D2 mediate myc-induced proliferation via sequestration of p27(Kip1) and p21(Cip1). EMBO J 1999;18:5310-20.

[29] Drayton S, Rowe J, Jones R, Vatcheva R, Cuthbert-Heavens D, Marshall J, et al. Tumor suppressor p16INK4a determines sensitivity of human cells to transformation by cooperating cellular oncogenes. Cancer Cell 2003;4:301-10.

[30] Grandori C, Wu KJ, Fernandez P, Ngouenet C, Grim J, Clurman BE, et al. Werner syndrome protein limits MYC-induced cellular senescence. Genes Dev 2003;17:1569-74.

[31] Fu L, Pelicano H, Liu J, Huang P, Lee C. The circadian gene Period2 plays an important role in tumor suppression and DNA damage response in vivo. Cell 2002;111:41-50.

[32] Matsuo T, Yamaguchi S, Mitsui S, Emi A, Shimoda F, Okamura H. Control mechanism of the circadian clock for timing of cell division in vivo. Science 2003;302:255-9.

[33] Lowe SW, Sherr CJ. Tumor suppression by Ink4a-Arf: progress and puzzles. Curr Opin Genet Dev 2003;13:77-83.

[34] Nobori T, Miura K, Wu DJ, Lois A, Takabayashi K, Carson DA. Deletions of the cyclin-dependent kinase-4 inhibitor gene in multiple human cancers. Nature 1994;368:753-6.

[35] Rheinwald JG, Hahn WC, Ramsey MR, Wu JY, Guo Z, Tsao H, et al. A two-stage, p16(INK4A)- and p53-dependent keratinocyte senescence mechanism that limits replicative potential independent of telomere status. Mol Cell Biol 2002;22:5157-72.

[36] Zhu J, Woods D, McMahon M, Bishop JM. Senescence of human fibroblasts induced by oncogenic Raf. Genes Dev 1998;12:2997-3007.

[37] Wang W, Chen JX, Liao R, Deng Q, Zhou JJ, Huang S, et al. Sequential activation of the MEK-extracellular signal-regulated kinase and MKK3/6-p38 mitogen-activated protein kinase pathways mediates oncogenic ras-induced premature senescence. Mol Cell Biol 2002;22:3389-403.

[38] Grandinetti KB, David G. Sin3B: an essential regulator of chromatin modifications at E2F target promoters during cell cycle withdrawal. Cell Cycle 2008;7:1550-4.

[39] Rayman JB, Takahashi Y, Indjeian VB, Dannenberg JH, Catchpole S, Watson RJ, et al. E2F mediates cell cycle-dependent transcriptional repression in vivo by recruitment of an HDAC1/mSin3B corepressor complex. Genes Dev 2002;16:933-47.

[40] Xie X, Rigor P, Baldi P. MotifMap: a human genome-wide map of candidate regulatory motif sites. Bioinformatics 2009;25:167-74.

[41] Kowalska E, Ripperger JA, Hoegger DC, Bruegger P, Buch T, Birchler T, et al. NONO couples the circadian clock to the cell cycle. Proc Natl Acad Sci U S A 2013;110:1592-9.

[42] Storcelova M, Vician M, Reis R, Zeman M, Herichova I. Expression of cell cycle regulatory factors hus1, gadd45a, rb1, cdkn2a and mre11a correlates with expression of clock gene per2 in human colorectal carcinoma tissue. Mol Biol Rep 2013;40:6351-61.

[43] Maier B, Kramer A. A NONO-gate times the cell cycle. Proc Natl Acad Sci U S A 2013;110:1565-6.

[44] Sherr CJ. Autophagy by ARF: a short story. Mol Cell 2006;22:436-7.

[45] Khan S, Guevara C, Fujii G, Parry D. p14ARF is a component of the p53 response following ionizing irradiation of normal human fibroblasts. Oncogene 2004;23:6040-6.

[46] Khan SH, Moritsugu J, Wahl GM. Differential requirement for p19ARF in the p53-dependent arrest induced by DNA damage, microtubule disruption, and ribonucleotide depletion. Proc Natl Acad Sci U S A 2000;97:3266-71.

[47] Moll UM, Petrenko O. The MDM2-p53 interaction. Mol Cancer Res 2003;1:1001-8.

[48] Weber JD, Taylor LJ, Roussel MF, Sherr CJ, Bar-Sagi D. Nucleolar Arf sequesters Mdm2 and activates p53. Nat Cell Biol 1999;1:20-6.

[49] Miki T, Matsumoto T, Zhao Z, Lee CC. p53 regulates Period2 expression and the circadian clock. Nat Commun 2013;4:2444.

[50] Zindy F, Eischen CM, Randle DH, Kamijo T, Cleveland JL, Sherr CJ, et al. Myc signaling via the ARF tumor suppressor regulates p53-dependent apoptosis and immortalization. Genes Dev 1998;12:2424-33.

[51] Polager S, Ginsberg D. p53 and E2f: partners in life and death. Nat Rev Cancer 2009;9:738-48.

[52] El-Deiry WS. The role of p53 in chemosensitivity and radiosensitivity. Oncogene 2003;22:7486-95.

[53] Sherr CJ, Roberts JM. CDK inhibitors: positive and negative regulators of G1-phase progression. Genes Dev 1999;13:1501-12.

[54] Harbour JW, Dean DC. The Rb/E2F pathway: expanding roles and emerging paradigms. Genes Dev 2000;14:2393-409.

[55] Robles SJ, Adami GR. Agents that cause DNA double strand breaks lead to p16INK4a enrichment and the premature senescence of normal fibroblasts. Oncogene 1998;16:1113-23.

[56] Forger DB, Peskin CS. A detailed predictive model of the mammalian circadian clock. Proc Natl Acad Sci U S A 2003;100:14806-11.

[57] Leloup JC, Goldbeter A. Toward a detailed computational model for the mammalian circadian clock. Proc Natl Acad Sci U S A 2003;100:7051-6.

[58] Mirsky HP, Liu AC, Welsh DK, Kay SA, Doyle FJ, 3rd. A model of the cell-autonomous mammalian circadian clock. Proc Natl Acad Sci U S A 2009;106:11107-12.
[59] Korencic A, Bordyugov G, Kosir R, Rozman D, Golicnik M, Herzel H. The interplay of cis-regulatory elements rules circadian rhythms in mouse liver. PLoS One 2012;7:e46835.
[60] Smolen P, Baxter DA, Byrne JH. A reduced model clarifies the role of feedback loops and time delays in the Drosophila circadian oscillator. Biophys J 2002;83:2349-59.
[61] Goodwin BC. Oscillatory behavior in enzymatic control processes. Adv Enzyme Regul 1965;3:425-38.
[62] Ruoff P, Vinsjevik M, Monnerjahn C, Rensing L. The Goodwin oscillator: on the importance of degradation reactions in the circadian clock. J Biol Rhythms 1999;14:469-79.
[63] Ang J, Ingalls B, McMillen D. Probing the input-output behavior of biochemical and genetic systems system identification methods from control theory. Methods Enzymol 2011;487:279-317.
[64] Sporl F, Schellenberg K, Blatt T, Wenck H, Wittern KP, Schrader A, et al. A circadian clock in HaCaT keratinocytes. J Invest Dermatol 2011;131:338-48.
[65] Serrano M, Lee H, Chin L, Cordon-Cardo C, Beach D, DePinho RA. Role of the INK4a locus in tumor suppression and cell mortality. Cell 1996;85:27-37.
[66] Benanti JA, Galloway DA. Normal human fibroblasts are resistant to RAS-induced senescence. Mol Cell Biol 2004;24:2842-52.
[67] Wong JV, Yao G, Nevins JR, You L. Viral-mediated noisy gene expression reveals biphasic E2f1 response to MYC. Mol Cell 2011;41:275-85.
[68] Hermeking H, Rago C, Schuhmacher M, Li Q, Barrett JF, Obaya AJ, et al. Identification of CDK4 as a target of c-MYC. Proc Natl Acad Sci U S A 2000;97:2229-34.
[69] Sears R, Leone G, DeGregori J, Nevins JR. Ras enhances Myc protein stability. Mol Cell 1999;3:169-79.
[70] Leone G, Sears R, Huang E, Rempel R, Nuckolls F, Park CH, et al. Myc requires distinct E2F activities to induce S phase and apoptosis. Mol Cell 2001;8:105-13.
[71] Sanada K, Okano T, Fukada Y. Mitogen-activated protein kinase phosphorylates and negatively regulates basic helix-loop-helix-PAS transcription factor BMAL1. J Biol Chem 2002;277:267-71.
[72] Relogio A, Thomas P, Medina-Perez P, Reischl S, Bervoets S, Gloc E, et al. Ras-mediated deregulation of the circadian clock in cancer. PLoS Genet 2014;10:e1004338.
[73] Faulk WP, Barabas K, Sun IL, Crane FL. Transferrin-adriamycin conjugates which inhibit tumor cell proliferation without interaction with DNA inhibit plasma membrane oxidoreductase and proton release in K562 cells. Biochem Int 1991;25:815-22.
[74] Elmore LW, Rehder CW, Di X, McChesney PA, Jackson-Cook CK, Gewirtz DA, et al. Adriamycin-induced senescence in breast tumor cells involves functional p53 and telomere dysfunction. J Biol Chem 2002;277:35509-15.
[75] Dibner C, Sage D, Unser M, Bauer C, d'Eysmond T, Naef F, et al. Circadian gene expression is resilient to large fluctuations in overall transcription rates. EMBO J 2009;28:123-34.
[76] Chen R, Schirmer A, Lee Y, Lee H, Kumar V, Yoo SH, et al. Rhythmic PER abundance defines a critical nodal point for negative feedback within the circadian clock mechanism. Mol Cell 2009;36:417-30.

[77] Levi F, Okyar A, Dulong S, Innominato PF, Clairambault J. Circadian timing in cancer treatments. Annu Rev Pharmacol Toxicol 2010;50:377-421.

Appendices

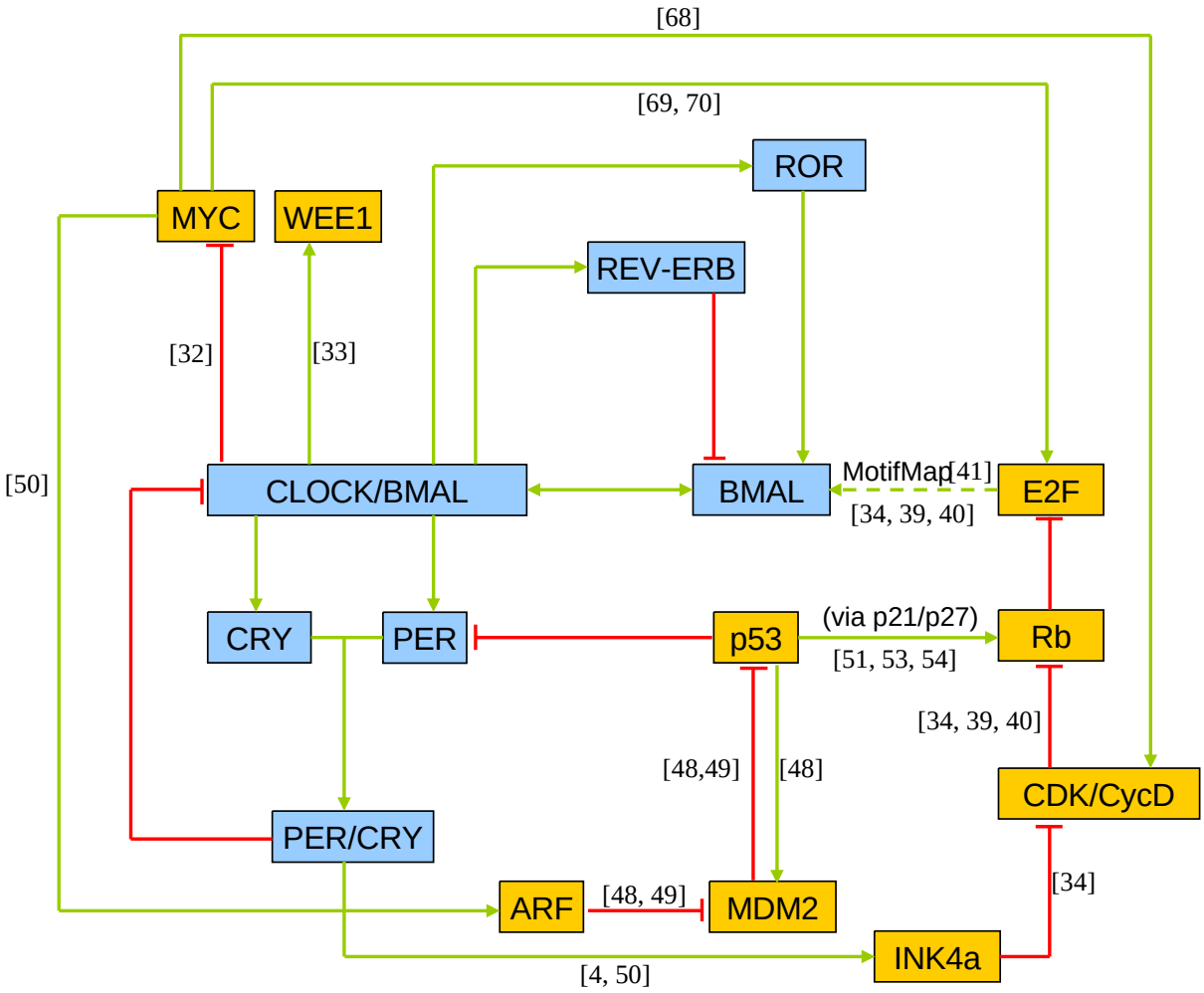

Figure S1: Simplified schematic diagram of the extended network with references for newly-added links marked. The species in blue boxes are components (including genes and proteins) already included in the pre-exsiting mathematical model for mammalian core circadian clock and the species in yellow boxes are newly added components in the extended model. For each newly-added link, the corresponding references are represented in square bracket.

Table S1: List of Variables. The extended model included 45 variables in total, out of which 20 are adapted from the original model.

Variable [a.u.]	Name	Note
x1	CLOCK/BMAL	*
x2	PER^*_N/CRY_N	*
x3	PER_N/CRY_N	*
PC	PER/CRY_{pool}	*
x5	$REV\text{-}ERB_N$	*
x6	ROR_N	*
x7	$INK4a_N$	
x8	ARF_N	
x9	$MDM2_N$	
x10	$p53_N$	
x11	$p53/MDM2_N$	
x12	$ARF/MDM2_N$	
x13	$INK4a_N$	
x14	$CDK/CycD_N$	
x15	$CDK/INK4a_N$	
x16	$E2F_N$	
x17	Rb_N	
x18	$RB\text{-}E2F_N$	
x19	RB^*_N	
x20	MYC_N	
y1	*Per*	*
y2	*Cry*	*
y3	*Rev-Erb*	*
y4	*Ror*	*
y5	*Bmal*	*
y6	*Ink4a*	
y7	*Arf*	
y8	*c-Myc*	
y9	*Wee1*	
y10	*Mdm2*	
y11	*CDK/CycD*	
y12	*E2F*	
z1	CRY_c	*
z2	PER_c	*
z3	PER^*_c	*
z4	PER^*_c/CRY_c	*
z5	PER_c/CRY_c	*
z6	$REV\text{-}ERB_c$	*
z7	ROR_c	*

(*Continued*)

Variable [a.u.]	Name	Note
z8	$BMAL_c$	*
z9	ARF_c	
z10	$MDM2_c$	
z11	$INK4a_c$	
z12	$CDK/CycD_c$	
z13	$E2F_c$	
z14	MYC_c	

* components included in the original model

Italic-written: mRNAs

"c"-indexed: cytoplasmic proteins

"N"-indexed: nuclear proteins

Table S2: List of parameters.

Parameters	Name	Value	Reference
Degradation rates for nuclear proteins or nuclear protein complexes [hour^{-1}]			
dx1	CLOCK/BMAL	0.08	[1]
dx2	PER^*_N/CRY_N	0.06	[1]
dx3	PER_N/CRY_N	0.09	[1]
dx5	$REV\text{-}ERB_N$	0.17	[1]
dx6	ROR_N	0.12	[1]
dx7	$BMAL_N$	0.15	[1]
dx8	ARF_N	0.11	[2]
dx9	$MDM2_N$	0.46	[3]
dx10	$p53_N$	0.231	[3]
dx11	$p53/MDM2_N$	2.07	[4]
dx12	$ARF/MDM2_N$	1.39	[3]
dx13	$INK4a_N$	0.11	[5]
dx14	$CDK/CycD_N$	1.5	[6, 7]
dx16	$E2F_N$	0.35	[8]
dx17	Rb_N	0.069	[9]
dx18	$Rb\text{-}E2F_N$	0.03	[10, 11]
dx19	Rb^*_N	0.069	[11, 12]
dx20	MYC_N	1.39	[13, 14]
Degradation rates for mRNAs [hour^{-1}]			
dy1	*Per*	0.3	[1]
dy2	*Cry*	0.2	[1]
dy3	*Rev-Erb*	2	[1]
dy4	*Ror*	0.2	[1]
dy5	*Bmal*	1.6	[1]
dy6	*Ink4a*	0.86[a]	
dy7	*Arf*	0.69	
dy8	*c-Myc*	0.86 [a]	
dy9	*Wee1*	0.86 [a]	
dy10	*Mdm2*	0.36	[15]
dy11	*CDK/CycD*	0.86 [a]	
dy12	*E2F*	0.25	
Degradation rates for cytoplasmic proteins [hour^{-1}]			
dz1	CRY_c	0.23	[1]
dz2	PER_c	0.25	[1]
dz3	PER^*_c	0.6	[1]
dz4	PER^*_c/CRY_c	0.2	[1]
dz5	PER_c/CRY_c	0.2	[1]
dz6	$REV\text{-}ERB_c$	0.31	[1]
dz7	ROR_c	0.3	[1]

(*Continued*)

dz8	$BMAL_c$	0.73	[1]
dz9	ARF_c	0.3525 [a]	
dz10	$MDM2_c$	0.3525 [a]	
dz11	$INK4a_c$	0.3525 [a]	
dz12	$CDK/CycD_c$	0.7	
dz13	$E2F_c$	0.7	
dz14	MYC_c	0.7	[16]
	Reaction rares for complex formation/dissociation		
kfx1	CLOCK/BMAL-complex formation	2.3	[1]
kdx1	CLOCK/BMAL-complex dissociation	0.01	[1]
kfz4	PER^*_c/CRY_c-complex formation	1	[1]
kdz4	PER^*_c/CRY_c-complex dissociation	1	[1]
kfz5	PER_c/CRY_c-complex formation	1	[1]
kdz5	PER_c/CRY_c-complex dissociation	1	[1]
kfx11	$p53/MDM2_N$-complex formation	3.96	
kdx11	$p53/MDM2_N$-complex dissociation	0.0396	
kfx12	$ARF/MDM2_N$-complex formation	8	
kdx12	$ARF/MDM2_N$-complex dissociation	0.0396	
kfx15	$INK4a/CDK4/CYCD_N$-complex formation	8	
kfx18	Rb/E2F-complex formation	18	
	Phosphorylation/dephosphorylation reaction rates [$hour^{-1}$]		
kphz2	PER_C phosphorylation rate	2	[1]
kdphz3	PER_C* dephosphorylation rate	0.05	[1]
kphx17	Rb phosphorylation rate	18	[11]
kdphx19	Rb* dephosphorylation rate	3.6	[11]
Kph	activation constant for Rb phosphorylation by CDK4/CYCD	0.92	[17]
Kdph	activation constant for Rb^* dephosphorylation	0.01	[18]
Kbp	inhibition constant for Rb phosphorylation by p53	0.2 [c]	
	Transcription rates [a.u. $hour^{-1}$]		
V_{1max}	*Per*	1	[1]
V_{2max}	*Cry*	2.92	[1]
V_{3max}	*Rev-Erb*	1.9	[1]
V_{4max}	*Ror*	10.9	[1]
V_{5max}	*Bmal*	1	[1]
V_{6max}	*Ink4a*	3.544 [a]	
V_{7max}	*Arf*	3.544 [a]	
V_{8max}	*c-Myc*	3.544 [a]	
V_{9max}	*Wee1*	3.544 [a]	
V_{10max}	*Mdm2*	5.4	[19]
	Activation/inhibition rates		
kt1	*Per* activation rate	3	[1]

(*Continued*)

ki1	*Per* inhibition rate	0.9	[1]
kt2	*Cry* activation rate	2.4	[1]
ki2	*Cry* inhibition rate	0.7	[1]
ki21	*Cry* inhibition rate	5.2	[1]
kt3	*Rev-Erb* activation rate	2.07	[1]
ki3	*Rev-Erb* inhibition rate	3.3	[1]
kt4	*Ror* activation rate	0.9	[1]
ki4	*Ror* inhibition rate	0.4	[1]
kt5	*Bmal* activation rate	8.35	[1]
ki5	*Bmal* inhibition rate	1.94	[1]
kii1	*Per* inhibition rate 2 (by p53)	2.488 [a]	
kt5_e	*Bmal* activation rate (by E2F)	5 [c]	
kt6	*Ink4a* activation rate	3.344 [a]	
kt7	*Arf* activation rate	3.344 [a]	
ki8	*c-Myc*-inhibition rate 1	2.488 [a]	
kii8	*c-Myc*-inhibition rate 2 (PC to CB)	2.488 [a]	
kt9	*Wee1* activation rate	3.344 [a]	
ki9	*Wee1* inhibition rate	2.488 [a]	
kt10	*Mdm2* activation rate	1.85	[19]
kt11	*Cdk4* activation rate	0.15 [c]	
kt12	*E2F* activation rate	3.344 [a]	
	Transcription fold activation (dimensionless)		
a	*Per*	12	[1]
d	*Cry*	12	[1]
g	*Rev-Erb*	5	[1]
h	*Ror*	5	[1]
i	*Bmal*	12	[1]
a_1	*Bmal* (by E2F)	3 [c]	
o	*Ink4a*	9.2 [a]	
l	*Arf*	9.2 [a]	
l1	*Wee1*	9.2 [a]	
r1	*Mdm2*	11	[19]
r2	*Cdk4*	9.2 [a]	
r3	*E2F*	9.2 [a]	
	Production rates [hour^{-1}]		
kp1	PER_c	0.4	[1]
kp2	CRY_c	0.26	[1]
kp3	$REV\text{-}ERB_c$	0.37	[1]
kp4	ROR_c	0.76	[1]
kp5	$BMAL_c$	1.21	[1]
kp6	$INK4a_c$	0.6 [a]	
kp7	ARF_c	0.6 [a]	

(*Continued*)

kp8	MYC_c	0.6 [a]	
kp10	$MDM2_c$	0.6 [a]	
kp11	$CDK4_c$	0.6 [a]	
kp12	$E2F_c$	0.4	
	Import/Export rates [hour^{-1}]		
kiz4	PER_c*/CRY_c	0.2	[1]
kiz5	PER_c/CRY_c	0.1	[1]
kiz6	REV-ERB_c	0.5	[1]
kiz7	ROR_c	0.1	[1]
kiz8	$BMAL_c$	0.1	[1]
kex2	PER_N*/CRY_N	0.02	[1]
kex3	PER_N/CRY_N	0.02	[1]
kiz10	$MDM2_c$	0.2 [a]	
kiz11	$INK4a_c$	0.2 [a]	
kiz9	ARF_c	0.2 [a]	
kiz12	$CDK4_c$	0.2 [a]	
kiz13	$E2F_c$	0.2 [a]	
kiz14	MYC_c	0.2 [a]	
	Hill coefficients of transcription (dimensionless)		
b	*Per*-activation	5	[1]
c	*Per*-inhibition	7	[1]
e	*Cry*-activation	6	[1]
f	*Cry*-inhibition	4	[1]
f1	*Cry*-inhibition	1	[1]
v	*Rev-Erb*-activation	6	[1]
w	*Rev-Erb*-inhibition	2	[1]
p	*Ror*-activation	6	[1]
q	*Ror*-inhibition	3	[1]
n	*Bmal*-activation	2	[1]
m	*Bmal*-inhibition	5	[1]
r	*Ink4a*-activation	1 [b]	
s	*Arf*-activation	1 [b]	
h4	*c-Myc*-inhibition-1	1 [b]	
h5	*c-Myc*-inhibition-2	1 [b]	
h6	*Wee1*-activation	1 [b]	
h7	*Wee1*-inhibition	1 [b]	
h1	*Mdm2*-activation	1.8	[20]
h8	*Per*-inhibition (by p53)	1 [b]	
a_2	*Bmal* (by E2F)	1 [b]	
h2	*Cdk4*-activation	1 [b]	
h3	*E2F*-activation	1 [b]	
	Exogenous RNA [a.u.]		

(*Continued*)

$y1_0$	*Per*	0	[1]
$y2_0$	*Cry*	0	[1]
$y3_0$	*Rev-Erb*	0	[1]
$y4_0$	*Ror*	0	[1]
$y5_0$	*Bmal*	0	[1]
Ink4a0	*Ink4a*	0 [a]	
Mdm0	*Mdm2*	0 [a]	
Arf0	*Arf*	0 [a]	
CDK0	*Cdk4*	0 [a]	
Myc0	*Myc*	0 [a]	
E2F0	*E2F*	0 [a]	
	Nuclear protein [a.u.]		
source_p53	p53	4.5 [c]	
source_Rb	Rb	1 [c]	

[a] average value of all parameters in the same category used in [1].

[b] the hill coefficients of new components was pre-set to 1 at this stage.

[c] parameters which were fine-tuned to maintain the oscillations of the system and to fit experimental observations.

References for Table S2

[1] Relogio A, Westermark PO, Wallach T, Schellenberg K, Kramer A, Herzel H. Tuning the mammalian circadian clock: robust synergy of two loops. PLoS Comput Biol 2011;7:e1002309.

[2] Kuo ML, den Besten W, Bertwistle D, Roussel MF, Sherr CJ. N-terminal polyubiquitination and degradation of the Arf tumor suppressor. Genes Dev 2004;18:1862-74.

[3] Zhang Y, Xiong Y, Yarbrough WG. ARF promotes MDM2 degradation and stabilizes p53: ARF-INK4a locus deletion impairs both the Rb and p53 tumor suppression pathways. Cell 1998;92:725-34.

[4] Finlay CA. The mdm-2 oncogene can overcome wild-type p53 suppression of transformed cell growth. Mol Cell Biol 1993;13:301-6.

[5] Chen X, Barton LF, Chi Y, Clurman BE, Roberts JM. Ubiquitin-independent degradation of cell-cycle inhibitors by the REGgamma proteasome. Mol Cell 2007;26:843-52.

[6] Bates S, Parry D, Bonetta L, Vousden K, Dickson C, Peters G. Absence of cyclin D/cdk complexes in cells lacking functional retinoblastoma protein. Oncogene 1994;9:1633-40.

[7] Diehl JA, Zindy F, Sherr CJ. Inhibition of cyclin D1 phosphorylation on threonine-286 prevents its rapid degradation via the ubiquitin-proteasome pathway. Genes Dev 1997;11:957-72.

[8] Helin K. Regulation of cell proliferation by the E2F transcription factors. Curr Opin Genet Dev 1998;8:28-35.

[9] Mihara K, Cao XR, Yen A, Chandler S, Driscoll B, Murphree AL, et al. Cell cycle-dependent regulation of phosphorylation of the human retinoblastoma gene product. Science 1989;246:1300-3.

[10] Buchler NE, Gerland U, Hwa T. Nonlinear protein degradation and the function of genetic circuits. Proc Natl Acad Sci U S A 2005;102:9559-64.

[11] Yao G, Lee TJ, Mori S, Nevins JR, You L. A bistable Rb-E2F switch underlies the restriction point. Nat Cell

Biol 2008;10:476-82.
[12] von Willebrand M, Zacksenhaus E, Cheng E, Glazer P, Halaban R. The tyrphostin AG1024 accelerates the degradation of phosphorylated forms of retinoblastoma protein (pRb) and restores pRb tumor suppressive function in melanoma cells. Cancer Res 2003;63:1420-9.
[13] Ramsay G, Evan GI, Bishop JM. The protein encoded by the human proto-oncogene c-myc. Proc Natl Acad Sci U S A 1984;81:7742-6.
[14] Gregory MA, Hann SR. c-Myc proteolysis by the ubiquitin-proteasome pathway: stabilization of c-Myc in Burkitt's lymphoma cells. Mol Cell Biol 2000;20:2423-35.
[15] Mendrysa SM, McElwee MK, Perry ME. Characterization of the 5' and 3' untranslated regions in murine mdm2 mRNAs. Gene 2001;264:139-46.
[16] Sears R, Leone G, DeGregori J, Nevins JR. Ras enhances Myc protein stability. Mol Cell 1999;3:169-79.
[17] Grafstrom RH, Pan W, Hoess RH. Defining the substrate specificity of cdk4 kinase-cyclin D1 complex. Carcinogenesis 1999;20:193-8.
[18] Kholodenko BN. Cell-signalling dynamics in time and space. Nat Rev Mol Cell Biol 2006;7:165-76.
[19] Leenders GB, Tuszynski JA. Stochastic and Deterministic Models of Cellular p53 Regulation. Front Oncol 2013;3:64.
[20] Weinberg RL, Veprintsev DB, Bycroft M, Fersht AR. Comparative binding of p53 to its promoter and DNA recognition elements. J Mol Biol 2005;348:589-96.

Table S3: Robustness analysis. -10%: 10% decrease in the parameter value; 10%: 10% increase in the parameter value; Tnew: new value for T after the perturbation; DT%: variation of the new period to the wild type value. The wild-type period is 23.65 h.

Parameter	-10%		10%	
	Tnew	DT%	Tnew	DT%
dx1	23.89	1.019	23.49	-0.693
dx2	23.85	0.846	23.52	-0.554
dx3	23.7	0.224	23.62	-0.144
dx5	24.04	1.653	23.19	-1.953
dx6	23.82	0.723	23.49	-0.698
dx7	23.66	0.059	23.64	-0.059
dx8	23.65	0	23.65	0
dx9	23.65	0.004	23.65	-0.004
dx10	23.65	0	23.65	0
dx11	23.65	0	23.65	0
dx12	23.65	0	23.65	0
dx13	23.65	-0.008	23.65	0.008
dx14	23.65	0	23.65	0
dx16	23.67	0.068	23.63	-0.068
dx17	23.65	0	23.65	0
dx18	23.65	0	23.65	0
dx19	23.65	0	23.65	0
dx20	23.67	0.072	23.64	-0.063
dy1	23.78	0.529	23.62	-0.14
dy2	23.66	0.03	23.65	-0.021
dy3	23.95	1.277	23.36	-1.209
dy4	23.82	0.706	23.49	-0.685
dy5	23.94	1.222	23.42	-0.989
dy6	23.64	-0.051	23.67	0.08
dy7	23.65	-0.004	23.65	0.004
dy8	23.67	0.072	23.64	-0.063
dy9	23.65	0	23.65	0
dy10	23.66	0.021	23.65	-0.021
dy11	23.67	0.093	23.64	-0.047
dy12	23.67	0.076	23.63	-0.08
dz1	23.66	0.0381	23.64	-0.038
dz2	23.65	-0.0085	23.65	0.008
dz3	23.67	0.0719	23.64	-0.051
dz4	23.68	0.1184	23.63	-0.076
dz5	23.65	-0.0085	23.65	0.013
dz6	23.82	0.7019	23.48	-0.702
dz7	23.75	0.4144	23.55	-0.406
dz8	24.04	1.649	23.33	-1.336
dz9	23.65	-0.004	23.65	0.004
dz10	23.65	0.013	23.65	-0.013
dz11	23.64	-0.047	23.66	0.059
dz12	23.67	0.076	23.64	-0.047

(*Continued*)

Parameter	-10%		10%	
	Tnew	DT%	Tnew	DT%
dz13	23.67	0.068	23.63	-0.068
dz14	23.66	0.055	23.64	-0.051
kfx1	23.77	0.5116	23.55	-0.427
kdx1	23.65	0.0085	23.65	-0.008
kfz4	23.65	-0.0211	23.66	0.021
kdz4	23.66	0.0381	23.64	-0.034
kfz5	23.65	0.0169	23.65	-0.017
kdz5	23.65	-0.0169	23.65	0.017
kfx11	23.65	-0.004	23.65	0
kdx11	23.65	0	23.65	0
kfx12	23.65	0	23.65	0
kdx12	23.65	0	23.65	0
kfx15	23.65	0.013	23.65	-0.013
kfx18	23.65	0.004	23.65	-0.004
kphz2	23.65	0.0042	23.65	-0.004
kdphz3	23.65	0	23.65	0
kphx17	23.63	-0.068	23.66	0.038
kdphx19	23.66	0.03	23.64	-0.042
Kph	23.65	0.017	23.65	-0.017
Kdph	23.65	0	23.65	0
Kbp	23.64	-0.03	23.66	0.021
V1max	23.7	0.224	23.6	-0.199
V2max	23.67	0.093	23.64	-0.063
V3max	23.48	-0.727	23.81	0.672
V4max	23.6	-0.199	23.68	0.131
V5max	23.57	-0.342	23.72	0.288
V6max	23.67	0.085	23.64	-0.051
V7max	23.65	0.004	23.65	-0.004
V8max	23.63	-0.068	23.67	0.063
V9max	23.65	0	23.65	0
V10max	23.64	-0.025	23.65	0.017
kt1	23.68	0.118	23.83	0.77
ki1	23.66	0.042	23.69	0.182
kt2	23.6	-0.199	23.69	0.186
ki2	23.77	0.486	23.61	-0.161
ki21	23.67	0.063	23.64	-0.051
kt3	24.01	1.522	23.55	-0.44
ki3	23.64	-0.034	23.66	0.03
kt4	23.64	-0.047	23.67	0.072
ki4	23.47	-0.753	23.69	0.165
kt5	23.68	0.14	23.61	-0.178
ki5	23.81	0.681	23.51	-0.6
kii1	23.65	0.004	23.65	-0.004
kt5_e	23.67	0.076	23.63	-0.072
kt6	23.64	-0.034	23.66	0.042
kt7	23.65	0	23.65	0

(*Continued*)

Parameter	-10%		10%	
	Tnew	DT%	Tnew	DT%
ki8	23.65	-0.004	23.65	0.004
kii8	23.65	0.004	23.65	-0.004
kt9	23.65	0	23.65	0
ki9	23.65	0	23.65	0
kt10	23.65	0.017	23.65	-0.017
kt11	23.66	0.03	23.65	-0.021
kt12	23.66	0.042	23.64	-0.038
a	23.67	0.101	23.63	-0.08
d	23.68	0.135	23.63	-0.097
g	23.32	-1.404	23.95	1.285
h	23.61	-0.186	23.68	0.118
i	23.59	-0.245	23.7	0.211
a_1	23.59	-0.266	23.71	0.233
o	23.67	0.076	23.64	-0.055
l	23.65	0	23.65	-0.004
l1	23.65	0	23.65	0
r1	23.65	-0.013	23.65	0.008
r2	23.64	-0.047	23.67	0.08
r3	23.64	-0.055	23.66	0.051
kp1	23.7	0.224	23.6	-0.199
kp2	23.67	0.093	23.64	-0.063
kp3	23.48	-0.727	23.81	0.672
kp4	23.6	-0.199	23.68	0.131
kp5	23.57	-0.342	23.72	0.288
kp6	23.67	0.085	23.64	-0.051
kp7	23.65	0.004	23.65	-0.004
kp8	23.63	-0.068	23.67	0.063
kp10	23.64	-0.025	23.65	0.017
kp11	23.64	-0.047	23.67	0.085
kp12	23.63	-0.097	23.67	0.08
kiz4	23.68	0.11	23.63	-0.106
kiz5	23.69	0.182	23.61	-0.161
kiz6	23.78	0.562	23.55	-0.423
kiz7	23.64	-0.051	23.65	0.008
kiz8	23.62	-0.144	23.67	0.085
kex2	23.68	0.14	23.62	-0.127
kex3	23.65	0.008	23.65	-0.008
kiz10	23.65	-0.017	23.65	0.013
kiz11	23.66	0.059	23.64	-0.042
kiz9	23.65	0.004	23.65	-0.004
kiz12	23.64	-0.047	23.67	0.068
kiz13	23.63	-0.076	23.67	0.063
kiz14	23.64	-0.051	23.66	0.047
b	23.65	-0.013	23.79	0.575
c	24	1.476	23.47	-0.753
e	23.63	-0.106	23.68	0.114

(*Continued*)

Parameter	-10%		10%	
	Tnew	DT%	Tnew	DT%
f	23.65	-0.021	23.67	0.063
f1	23.65	-0.017	23.65	0.013
v	23.41	-1.006	23.83	0.748
w	23.57	-0.33	23.71	0.254
p	23.66	0.03	23.64	-0.025
q	23.74	0.381	23.34	-1.332
n	23.75	0.44	23.56	-0.389
m	23.19	-1.928	24.05	1.674
r	23.65	-0.004	23.65	0.017
s	23.65	-0.004	23.65	0.004
h4	23.65	-0.017	23.65	0.017
h5	23.65	-0.008	23.65	0.004
h6	23.65	0	23.65	0
h7	23.65	0	23.65	0
h1	23.66	0.021	23.65	-0.021
h8	23.65	0.008	23.65	-0.008
a_2	23.65	-0.017	23.65	0.017
h2	23.65	-0.017	23.65	0.017
h3	23.67	0.08	23.63	-0.085
source_p53	23.65	0.017	23.65	-0.017
source_Rb	23.65	0.008	23.65	-0.008

Table S4: Ordinary differential equations for core-clock components [1].

	ODEs	
CLOCK/BMAL	$\frac{dx1}{dt} = kf_{x1}x7 - kd_{x1}x1 - d_{x1}x1$	(1)
Rev-Erb	$\frac{dy3}{dt} = V_{3max}\frac{1 + g\left(\frac{x1}{k_{t3}}\right)^{v}}{1 + \left(\frac{PC}{k_{i3}}\right)^{w}\left(\frac{x1}{k_{t3}}\right)^{v} + \left(\frac{x1}{k_{t3}}\right)^{v}} - d_{y3}y3$	(2)
Ror	$\frac{dy4}{dt} = V_{4max}\frac{1 + h\left(\frac{x1}{k_{t4}}\right)^{p}}{1 + \left(\frac{PC}{k_{i4}}\right)^{w}\left(\frac{x1}{k_{t4}}\right)^{v} + \left(\frac{x1}{k_{t4}}\right)^{v}} - d_{y4}y4$	(3)
REV-ERB$_c$	$\frac{dz6}{dt} = k_{p3}(y3 + y3_0) - ki_{z6}z6 - d_{z6}z6$	(4)
ROR$_c$	$\frac{dz7}{dt} = k_{p4}(y4 + y4_0) - ki_{z7}z7 - d_{z7}z7$	(5)
REV-ERB$_N$	$\frac{dx5}{dt} = ki_{z6}z6 - d_{x5}x5$	(6)
ROR$_N$	$\frac{dx6}{dt} = ki_{z7}z7 - d_{x6}x6$	(7)
Bmal	$\frac{dy5}{dt} = V_{5max}\frac{1 + i\left(\frac{x6}{k_{t5}}\right)^{n}}{1 + \left(\frac{x5}{k_{i5}}\right)^{m} + \left(\frac{x6}{k_{t5}}\right)^{n}} - d_{y5}y5$	(8)
BMAL$_c$	$\frac{dz8}{dt} = k_{p5}(y5 + y5_0) - ki_{z8}z8 - d_{z8}z8$	(9)
BMAL$_N$	$\frac{dx7}{dt} = ki_{z8}z8 + kd_{x1}x1 - kf_{x1}x7 - d_{x7}x7$	(10)
Per	$\frac{dy1}{dt} = V_{1max}\frac{1 + a\left(\frac{x1}{k_{t1}}\right)^{b}}{1 + \left(\frac{PC}{k_{i1}}\right)^{c}\left(\frac{x1}{k_{t1}}\right)^{b} + \left(\frac{x1}{k_{t1}}\right)^{b}} - d_{y1}y1$	(11)
Cry	$\frac{dy1}{dt} = V_{1max}\frac{1 + a\left(\frac{x1}{k_{t1}}\right)^{b}}{1 + \left(\frac{PC}{k_{i1}}\right)^{c}\left(\frac{x1}{k_{t1}}\right)^{b} + \left(\frac{x1}{k_{t1}}\right)^{b}} - d_{y1}y1$	(12)
CRY$_c$	$\frac{dz1}{dt} = k_{p2}(y2 + y2_0) + kd_{z4}z4 + kd_{z5}z5 - kf_{z5}z1z2 - kf_{z4}z1z3 - d_{z1}z1$	(13)
PER$_c$	$\frac{dz2}{dt} = k_{p1}(y1 + y1_0) + kd_{z5}z5 + kd_{phz3}z3 - kf_{z5}z2z1 - kph_{z2}z2 - d_{z2}z2$	(14)
PER$_c$*	$\frac{dz3}{dt} = kph_{z2}z2 + kd_{z4}z4 - kd_{phz3}z3 - kf_{z4}z3z1 - d_{z3}z3$	(15)

(*Continued*)

PER_c*/ CRY_c	$\frac{dz4}{dt} = kf_{z4}z1z3 + ke_{x2}x2 - ki_{z4}z4 - kd_{z4}z4 - d_{z4}z4$	(16)
PER_c/ CRY_c	$\frac{dz5}{dt} = kf_{z5}z1z2 + ke_{x3}x3 - ki_{z5}z5 - kd_{z5}z5 - d_{z5}z5$	(17)
PER_N*/ CRY_N	$\frac{dx2}{dt} = ki_{z4}z4 - ke_{x2}x2 - d_{x2}x2$	(18)
PER_N/ CRY_N	$\frac{dx2}{dt} = ki_{z4}z4 - ke_{x2}x2 - d_{x2}x2$	(19)
PER/ CRY_{pool}	$PC = x2 + x3$	(20)

[1] Relogio A, Westermark PO, Wallach T, Schellenberg K, Kramer A, Herzel H. Tuning the mammalian circadian clock: robust synergy of two loops. PLoS Comput Biol 2011;7:e1002309.